

# Quantum error mitigation for fault-tolerant quantum computing

Yasunari Suzuki,<sup>1,2,\*</sup> Suguru Endo,<sup>1,†</sup> Keisuke Fujii,<sup>3,4,5</sup> and Yuuki Tokunaga<sup>1,‡</sup>

<sup>1</sup>*NTT Secure Platform Laboratories, NTT Corporation, Musashino 180-8585, Japan*

<sup>2</sup>*JST, PRESTO, 4-1-8 Honcho, Kawaguchi, Saitama, 332-0012, Japan*

<sup>3</sup>*Graduate School of Engineering Science, Osaka University,*

*1-3 Machikaneyama, Toyonaka, Osaka 560-8531, Japan*

<sup>4</sup>*Center for Quantum Information and Quantum Biology,*

*Institute for Open and Transdisciplinary Research Initiatives, Osaka University, Japan*

<sup>5</sup>*Center for Emergent Matter Science, RIKEN, Wako Saitama 351-0198, Japan*

Fault-tolerant quantum computing (FTQC) is a form of universal quantum computing that suppresses physical errors via quantum error correction (QEC). Although the effective error rate decreases exponentially with the code distance, it is expected that the number of available physical qubits and the  $T$ -gate count will be restricted in the early years of FTQC. Meanwhile, quantum error mitigation (QEM) was recently introduced for suppressing errors in noisy intermediate-scale quantum (NISQ) devices; it improves the computation accuracy of near-term quantum algorithms with its overhead being a greater number of samples. In this work, we integrate QEC and QEM into an efficient FTQC architecture that effectively increases the code distance and  $T$ -gate count. This scheme will dramatically alleviate the required overheads of FTQC for achieving high-accuracy quantum computing.

## I. INTRODUCTION

Quantum computers are believed to be capable of implementing several tasks such as factoring and Hamiltonian simulations, in exponentially smaller computational times than those of classical computers [1, 2]. However, quantum systems generally interact with their environments, which leads to physical errors in the system that may destroy their quantum advantage. Since the physical error rates of quantum computers are still much higher than those of classical computers, it is vital to suppress these errors.

As a solution, fault-tolerant quantum computing (FTQC) using quantum error-correcting codes has been studied [3–7]. Here, information is encoded into a logical code space constructed from several noisy physical qubits. It has been shown that the effective error probability can be made arbitrarily small by increasing the number of physical qubits as long as the error probabilities of the physical qubits are smaller than a certain threshold determined by the code. Note that the overhead of FTQC is the number of qubits, which increases polynomially with the code distance. Consequently, the number of necessary physical qubits is estimated to reach a few hundred thousand to several millions for solving practical problems such as Hamiltonian simulations and postclassical factoring [8, 9], which seems decades away, considering the current technology.

On the other hand, quantum error mitigation (QEM) has been proposed as an alternative way of dealing with

errors [10–19]. In particular, QEM is used to mitigate physical errors in noisy intermediate-scale quantum (NISQ) devices and improve the computation accuracy of near-term quantum algorithms such as the variational quantum eigensolver [19–24]. Without QEM, the error probabilities of NISQ devices are too high and the obtained results are quite unreliable. QEM relies on post-processing of the measurement outcomes and recovers the expectation values of the observables measured on quantum processors; hence it does not require encoding of qubits. Instead, QEM necessitates a greater sample number as an overhead, which generally increases exponentially with the number of error events in the quantum circuit.

As quantum technologies become mature and the qubit count increases, it is expected that the post-NISQ era will arrive. Moreover, there will be a transitional period from small-scale FTQC devices with a restricted number of qubits to fully scalable devices. The early FTQC devices in this period will be similar to the current NISQ devices in that the number of qubits will be restricted, and the quantum computers may be short of code distance and  $T$ -gate count to achieve the required accuracy, e.g., for chemistry calculations.

To solve this problem, we propose and analyze a framework for FTQC, where QEC and QEM are combined on an equal footing. We investigate how QEM should be incorporated in an architecture of FTQC and show that a more accurate expectation value can be calculated with a similar hardware requirement by QEM. Specifically, we show that probabilistic error cancellation, a QEM technique proposed by Temme *et al.* [10], can significantly improve the computation accuracy of FTQC. Our method mitigates two dominant error types: decoding errors due to insufficient code distances and approximation errors induced by the Solovay-Kitaev decomposition [25, 26], which we will simply call decoding errors and approx-

\* yasunari.suzuki.gz@hco.ntt.co.jp

† suguru.endo@hco.ntt.co.jp; Y.S and S.E contributed to this work equally

‡ yuuki.tokunaga.bf@hco.ntt.co.jp

imation errors throughout this paper. Note that there are crucial problems for performing probabilistic error cancellation on these two error types in the logical space, which we solved in the affirmative way. First, to apply probabilistic error cancellation, we need a good characterization of the noise model to compute QEM operations for a noise map. We show that decoding errors can be described with the stochastic logical Pauli error, which can be efficiently characterized with gate-set tomography on the code space [27, 28]. As well, the approximation errors of the Solovay-Kitaev algorithm can be characterized efficiently on classical computers. Second, the recovery operations of the probabilistic error cancellation must be compatible with the architecture of FTQC, such as gate teleportation with magic states and Pauli frame. To cope with noisy syndrome measurements and restricted transversal operations, several techniques, such as the Pauli frame and magic-state distillation, are employed in FTQC. It is not a trivial problem whether we can perform probabilistic error cancellation along with these techniques or not. We show that the recovery operations for these two types of errors can be properly constructed in FTQC. Also, since most of the error mitigation operations can be done only with virtual Pauli operations by updating the Pauli frame, there are negligible overheads on FTQC procedure except for the sampling overheads.

This paper is organized as follows. In Sec. II, we review probabilistic error cancellation and the architecture of fault-tolerant quantum computing. In Sec. III, we describe how to evaluate decoding errors and approximation errors. Then we show our novel FTQC architecture with an analytical argument of the cost of QEM and explain the effect of model estimation errors. In Sec. IV, we numerically analyze the sampling cost of QEM for decoding errors and approximation errors and demonstrate that we can effectively increase the code distance and the number of  $T$ -gates via QEM even when there are finite estimation errors. Finally, we conclude our paper with a discussion in Sec. V.

## II. PRELIMINARIES

### A. Quantum error mitigation and probabilistic error cancellation

There generally exist physical noises in quantum processors, which should be mitigated to obtain correct results. For simplicity, here we assume gate errors are Markovian, i.e., a noise process  $\mathcal{N}$  for a gate is totally independent of other gate errors. In this case, we have

$$\rho_{\text{out}} = \mathcal{N}_{N_G} \circ \mathcal{U}_{N_G} \circ \mathcal{N}_{N_G-1} \circ \mathcal{U}_{N_G-1} \cdots \mathcal{N}_1 \circ \mathcal{U}_1(\rho_{\text{in}}), \quad (1)$$

where  $\rho_{\text{out}}$  and  $\rho_{\text{in}}$  are the output and input quantum states,  $\mathcal{U}_k$  and  $\mathcal{N}_k$  denote the ideal and noisy part of the process of the  $k$ -th gates, and  $N_G$  is the number of gates.

To have the correct computation results, it is necessary to mitigate the effect of  $\mathcal{N}_k$ , ( $k = 1, 2, \dots, N_G$ ) to obtain

$$\rho_{\text{out}}^{\text{ideal}} = \mathcal{U}_{N_G} \circ \mathcal{U}_{N_G-1} \cdots \circ \mathcal{U}_1(\rho_{\text{in}}). \quad (2)$$

Quantum error mitigation (QEM) is proposed as a method for suppressing errors without encoding, which is useful especially for NISQ devices with a restricted number of qubits [10–12]. Generally, QEM methods recover not the ideal density matrix  $\rho_{\text{out}}^{\text{ideal}}$  itself, but the ideal expectation value of an observable  $\langle \hat{M} \rangle_{\text{ideal}} = \text{Tr}(\rho_{\text{out}}^{\text{ideal}} \hat{M})$  via classical post-processing. Note that QEM is not a scalable technique because the cost for QEM needs exponentially increasing circuit runs with the number of error events in the quantum circuit [10, 12].

Now we explain probabilistic error cancellation with which we can eliminate a bias of an expectation value of observables completely given the complete information of the noise model [10, 12]. We will apply this method to suppress errors in FTQC later. First, we identify the noise map  $\mathcal{N}$  via either process or gate set tomography [27, 28], and calculate the inverse  $\mathcal{N}^{-1}$ . Then, by finding a set of processes  $\{\mathcal{B}_i\}$  such that  $\mathcal{N}^{-1} = \sum_i \eta_i \mathcal{B}_i$  where  $\eta_i \in \mathbb{R}$  and  $\sum_i \eta_i = 1$ , we have

$$\begin{aligned} \mathcal{U} &= \mathcal{N}^{-1} \mathcal{N} \mathcal{U} \\ &= \sum_i \eta_i \mathcal{B}_i \mathcal{N} \mathcal{U}. \end{aligned} \quad (3)$$

We remark that the linear combination of tensor products of single-qubit Clifford operations and Pauli measurements can represent arbitrary operations [12]. We can rewrite Eq. (3) as

$$\mathcal{U} = \gamma_Q \sum_i q_i \text{sgn}(\eta_i) \mathcal{B}_i \mathcal{N} \mathcal{U}, \quad (4)$$

where  $\gamma_Q = \sum_i |\eta_i|$ ,  $q_i = \frac{|\eta_i|}{\gamma_Q}$ ,  $\gamma_Q \geq 1$  and  $\text{sgn}(\eta_i)$  is a parity which takes  $\pm 1$ , corresponding to the operation  $\mathcal{B}_i$ . We refer to as  $\gamma_Q$  as QEM cost because it is related to sampling overhead.

Now suppose we measure an observable  $\hat{M}$  and obtain

$$\langle \hat{M} \rangle_{\mathcal{U}} = \gamma_Q \sum_i q_i \langle \hat{\mu}_i^{\text{eff}} \rangle. \quad (5)$$

Here,  $\hat{\mu}_i^{\text{eff}} = \text{sgn}(\eta_i) \hat{m}_i$ , and  $\hat{m}_i$  is a measurement outcome for a process  $\mathcal{B}_i \mathcal{N} \mathcal{U}$ . We generate the process  $\mathcal{B}_i$  with a probability  $q_i$  and multiply the corresponding parity to the measurement result, which is denoted as  $\hat{\mu}_i^{\text{eff}}$ . Then the expectation value of the random variable  $\hat{\mu}^{\text{mit}} = \gamma_Q \hat{\mu}^{\text{eff}}$  approximates the error-free expectation value  $\langle \hat{M} \rangle_{\mathcal{U}}$ . Note that since  $\text{Var}[\hat{\mu}^{\text{mit}}] = \gamma_Q^2 \text{Var}[\hat{\mu}^{\text{eff}}]$  and a measurement outcome without QEM which we denote  $\hat{\mu}^{\text{mit}}$  has a similar variance, the variance of error-mitigated value is approximately amplified with  $\Gamma_Q = \gamma_Q^2$ . Therefore we need to have  $\Gamma_Q$  times more samples to achieve a similar accuracy before applying QEM.

In practice, probabilistic error cancellation is employed in a quantum circuit. The ideal process of the entire quantum circuit is described as  $\prod_{k=1}^{N_G} \mathcal{U}_k$ . Denoting  $\mathcal{U}_k = \gamma_Q^{(k)} \sum_{i_k} q_{i_k} \text{sgn}(\eta_{i_k}) \mathcal{B}_{i_k} \mathcal{N}_k \mathcal{U}_k$ , we have

$$\prod_{k=1}^{N_G} \mathcal{U}_k = \prod_{k=1}^{N_G} \gamma_Q^{(k)} \sum_{i_1 i_2 \dots i_{N_G}} \prod_{k=1}^{N_G} q_{i_k} \prod_{k=1}^{N_G} \text{sgn}(\eta_{i_k}) \prod_{k=1}^{N_G} \mathcal{B}_{i_k} \mathcal{N}_k \mathcal{U}_k. \quad (6)$$

From Eq. (6), we can see that in each gate we generate a process  $\mathcal{M}_{i_k}$  with probability  $q_{i_k}$ , and multiply the product of parities  $\prod_{k=1}^{N_G} \text{sgn}(\eta_{i_k})$  to the measurement results to obtain the outcome  $\hat{\mu}^{\text{eff}}$ . This procedure is repeated, and the product of the mean of outcomes  $\langle \hat{\mu}^{\text{eff}} \rangle$  and  $\gamma_Q^{\text{tot}} = \prod_{k=1}^{N_G} \gamma_Q^{(k)}$  approximates the correct expectation value. Note that now  $\gamma_Q^{\text{tot}}$  is the QEM cost for the entire quantum circuit. Let us assume the cost for each gate is uniform and can be approximated as  $\gamma_Q^{(k)} = \gamma_Q = 1 + a\varepsilon$  with  $a$  and  $\varepsilon$  being a positive constant value and an effective error rate, respectively. Now the QEM cost and the sampling overhead can be approximated as  $\gamma_Q^{\text{tot}} \simeq e^{a\varepsilon N_G} = e^{(\gamma_Q - 1)N_G}$  and  $\Gamma_Q^{\text{tot}} = (\gamma_Q^{\text{tot}})^2$ , which increase exponentially with the mean number of error events in the quantum circuit  $\varepsilon N_G$ . Note that for  $\varepsilon N_G = O(1)$  and  $\varepsilon \rightarrow 0$ , since  $\varepsilon^k N_G = 0$  ( $k \geq 2$ ), the QEM cost can be exactly described as  $\gamma_Q^{\text{tot}} = e^{(\gamma_Q - 1)N_G}$ .

## B. Fault-tolerant quantum computing

### 1. Stabilizer formalism

In a framework of fault-tolerant quantum computing (FTQC), we prepare a redundant number of physical qubits and perform quantum computing in a code space defined as a subspace of the whole Hilbert space. By repetitively performing quantum error detection and correction, we can protect logical qubits defined in a code space against physical errors. A state of logical qubits is manipulated in a fault-tolerant manner with a set of logical operations.

Stabilizer formalism [3, 29] is the most standard way to construct quantum error-correcting codes. When we construct  $k$  logical qubits with  $n$  physical qubits, a  $2^k$ -dimension code space  $\mathcal{C}$  is specified with a subgroup of  $n$ -qubit Pauli operators called stabilizer group. Let  $n$ -qubit Pauli group be

$$\mathcal{G}_n = \{\pm 1, \pm i\} \times \{I, X, Y, Z\}^{\otimes n}, \quad (7)$$

where  $I$  is an identity operator and  $X = \begin{pmatrix} 0 & 1 \\ 1 & 0 \end{pmatrix}$ ,  $Y = \begin{pmatrix} 0 & -i \\ i & 0 \end{pmatrix}$ ,  $Z = \begin{pmatrix} 1 & 0 \\ 0 & -1 \end{pmatrix}$  are Pauli operators. A set of Pauli operator  $\mathcal{S} \subset \mathcal{G}_n$  is called stabilizer group if  $\mathcal{S}$  is a commutative subgroup, the number of elements in  $\mathcal{S}$  is  $2^{n-k}$ , and  $-I \notin \mathcal{S}$ . We denote a  $(n-k)$  generator set of stabilizer group as  $\mathcal{G} = (g_1, \dots, g_{n-k})$ . The

code space  $\mathcal{C}$  is defined as an eigenspace with  $+1$  eigenvalues of all the operators in a stabilizer group, i.e.,  $\mathcal{C} = \{|\psi\rangle \mid \forall s_i \in \mathcal{S}, s_i |\psi\rangle = |\psi\rangle\}$ . In the code space, we can introduce logical basis as  $\{|0\rangle_L, |1\rangle_L\}^{\otimes k}$  and logical Pauli operators as  $\{I_L, X_L, Y_L, Z_L\}^{\otimes k}$ . A code distance  $d$  is defined as the minimum number of physical qubits on which an arbitrary logical operator except logical identity  $I_L^{\otimes k}$  acts.

During quantum computation, physical errors that occur on the encoded state are detected by  $(n-k)$  Pauli measurements  $P_s = \frac{1}{2}(I + (-1)^s g_i)$  for  $s \in \{0, 1\}$ . These measurements are called stabilizer measurements and their binary outcomes  $s$  are called syndrome values. The original state is restored by applying appropriate feedback operations that are estimated from syndrome values. These stabilizer measurements are performed repeatedly during computation. One repetition of the stabilizer measurements is called a code cycle of fault-tolerant quantum computing. If an effective error probability per physical qubit during a cycle is smaller than a certain threshold, we can estimate a Pauli operator that restores the original state with an exponentially small failure probability with the code distance  $d$ . Since the required number of physical qubit  $n$  increases polynomially to the code distance  $d$  in typical quantum error-correcting codes, we can exponentially decrease the error probability of logical qubits with polynomial qubit overhead.

### 2. Logical operations

We need to not only correct physical errors but also update a logical quantum state for computation. To this end, a universal set of logical operations should be done in a fault-tolerant manner. According to Solovay-Kitaev theorem [25, 26], we can approximate an arbitrary one- and two-qubit gates with a finite set of local operations.

For example, a set of Hadamard gate  $H = \frac{1}{\sqrt{2}} \begin{pmatrix} 1 & 1 \\ 1 & -1 \end{pmatrix}$ , controlled-not (CNOT) gate  $\Lambda = |0\rangle\langle 0| \otimes I + |1\rangle\langle 1| \otimes X$ , and  $T$ -gate  $T = \exp(i\frac{\pi}{8}Z)$  is a universal gate set. Several logical operations can be done by transversally operating the same one- or two-qubit operations on physical qubits. Since transversal operations increase an effective physical error rate per qubit during a cycle constantly, we can fault-tolerantly achieve transversal logical operations. However, it is known that there is no stabilizer code of which the set of transversal gates is universal [30]. Thus, we need an additional technique to achieve fault-tolerant and universal quantum computing. The most promising solution is to create a quantum state called a magic state and achieving non-transversal logical operations with gate teleportation [5]. For example,  $|A\rangle_L = TH|0\rangle_L = \frac{1}{\sqrt{2}}(e^{i\pi/8}|0\rangle_L + e^{-i\pi/8}|1\rangle_L)$  is a typical magic state and can be used for performing  $T$ -gate by consuming this state. This magic state encoded in a logical qubit can be constructed with a process called magic

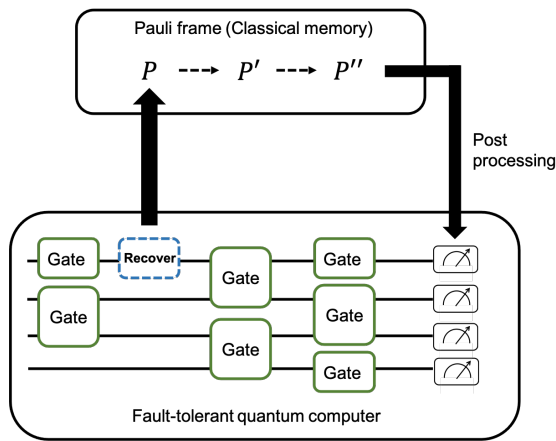


FIG. 1. Schematic figure of Pauli frame. The recovery operations are not physically applied on quantum computers but are stored on Pauli frame and efficiently updated after each Clifford gate operation. Depending on the state of the Pauli frame, measurement outcomes are flipped.

state injection. While the infidelity of a magic state created by magic state injection is generally larger than a logical error rate, we can utilize magic state distillation to create a high-fidelity magic state from several noisy magic states only with fault-tolerant logical operations and measurements. Since the application of  $T$ -gates requires a longer time than the other operations, the number of  $T$ -gates is one of the most dominant factors of the whole computation time of FTQC.

Although we can estimate a Pauli operation for recovery from syndrome values, we do not directly apply it immediately after estimation. Instead, we store what Pauli operations should be applied to physical qubits for recovery in a classical memory called Pauli frame [5, 31]. The stored operations will be taken into account when we perform logical measurements; the outcome of logical measurements is flipped according to the Pauli frame. The schematic figure is shown in Fig. 1. In the above construction of logical operations, the whole process except magic state injection consists only of Clifford operations and Pauli channels in a code space. Since a Pauli operator conjugated by a Clifford operator is also a Pauli operator, we can always track a recovery operator as a Pauli operator during computation. In addition, when we apply a logical Pauli operator to a quantum state, we can perform it only by updating a Pauli frame since a logical Pauli operator is a transversal physical Pauli operation. As far as classical computers are reliable, this operation is effectively noiseless.

### III. QUANTUM ERROR MITIGATION FOR FAULT-TOLERANT QUANTUM COMPUTING

In this section, we discuss how to apply QEM to FTQC. Here we consider two types of errors in FTQC:

decoding errors due to failure of error estimation and approximation errors in Solovay-Kitaev decomposition. First, we explain how these errors in FTQC can be modeled in Sec. III A. Then, we discuss how these errors can be canceled and evaluate their QEM costs in Sec. III B. Probabilistic error cancellation requires errors are estimated in advance. We also discuss the effect of estimation errors in probabilistic error cancellation and efficiency of characterization in Sec. III C.

#### A. Errors in fault-tolerant quantum computing

##### 1. Decoding error

Here we describe noise due to decoding failures. The first obstacle to applying probabilistic error cancellation to FTQC is how to characterize an effective map of noise due to decoding failures. If we suppose that the physical errors can be modeled as a stochastic physical Pauli map and assume that there are no errors on the ancillary qubits for syndrome measurements, we can define a logical noise map for decoding errors that is Markovian and a logical stochastic Pauli map. Yet, these assumptions do not hold in practice. Nevertheless, here we will assume that we can define an effectively Markovian logical error map for each logical operation and also assume that this noise map is a stochastic logical Pauli map. It is known that even if noise is unitary, a noise map in a logical space can be well approximated as stochastic Pauli noise when the code distance is sufficiently large [32]. Furthermore, the remaining coherent errors can be canceled by using pulse optimization techniques. Thus, it is reasonable to suppose that the decoding errors are almost stochastic Pauli errors. In addition, we numerically verified that we can regard the decoding errors as Markovian errors even in the presence of syndrome measurements. See Appendix F for the details.

Under the above assumptions, we can describe a noise map for a  $m$ -qubit logical operation  $\mathcal{N}_{\text{dec}}$  as the following stochastic Pauli noise:

$$\mathcal{N}_{\text{dec}}(\rho) = \sum_{g \in \{I_L, X_L, Y_L, Z_L\}^{\otimes m}} p_g g \rho g^\dagger, \quad (8)$$

where  $p_g \in \mathbb{R}$ ,  $\sum_g p_g = 1$  and  $p_g \geq 0$ . The sum of probabilities of non-identity logical operation is called a logical error probability  $p_{\text{dec}}$ , i.e.,  $p_{\text{dec}} = \sum_{g \neq I^{\otimes m}} p_g$ . It is known that when physical error rate  $p$  is smaller than a value called threshold  $p_{\text{th}}$ , an effective logical error probability per syndrome-measurement cycle  $p_{\text{cyc}}$  decreases exponentially to a code distance  $d$  as

$$p_{\text{cyc}} \simeq C_1 \left( C_2 \frac{p}{p_{\text{th}}} \right)^{(d+1)/2}, \quad (9)$$

where  $C_1, C_2$  are constants [33]. While the constant values depend on details of error correction schemes,  $C_1 \simeq 0.13$  and  $C_2 \simeq 0.61$  are expected in the typical

construction of surface codes and noise model [33, 34]. Suppose that a logical operation requires  $m$  cycles, then the logical error probability for the logical operation can be approximated as  $p_{\text{dec}}$  as

$$p_{\text{dec}} = 1 - (1 - p_{\text{cyc}})^m \simeq mp_{\text{cyc}}. \quad (10)$$

Note that the number of cycles per logical gate increases at most linearly with code distance  $d$ .

In the application of probabilistic error cancellation, we need to know logical error probabilities  $\{p_g\}$  in advance. While we can estimate  $\{p_g\}$  by gate-set tomography in logical space, the estimation results are not exact. The effect of estimation errors is discussed in Sec. III C and efficiency of our proposal including noise characterization is discussed in Sec. C.

## 2. Approximation error

Since we are only allowed to use a limited set of logical operations for achieving fault-tolerance, we need to decompose an arbitrary unitary gate to a sequence of available gates. Any unitary operator can be decomposed into a product of CNOT gates and single-qubit gates. Thus, we need to approximate single-qubit gates with a given gate set to a desired accuracy. With an improved Solovay-Kitaev algorithm [35], given a universal gate set such as  $\{T, H, S\}$ , single-qubit gate  $U$ , we can construct an approximated gate  $\tilde{U}$  which satisfies  $\varepsilon = \|\tilde{U} - U\|$  to an arbitrary accuracy  $\varepsilon$  as a sequence of given gate set with length  $\tilde{O}(\log(\varepsilon^{-1}))$  with  $\|\cdot\|$  being an operator norm. The error of approximated map is given by

$$\mathcal{N}_{\text{SK}}(\rho) = \tilde{U}U^\dagger \rho U\tilde{U}^\dagger. \quad (11)$$

Since this decomposition involves only single-qubit operations, this error channel can be efficiently and exactly evaluated in advance.

## B. Quantum error mitigation for fault-tolerant quantum computing

### 1. Overview of our framework

Here, we discuss that decoding errors and approximation errors can be mitigated with probabilistic error cancellation. When we insert recovery operations for probabilistic error cancellation, it is assumed that noise level of recovery operations for QEM are much lower than that of the error-mitigated gates. In NISQ computing, for example, it is natural to assume error probabilities of two-qubit gates are much larger than single-qubit gates and measurements; therefore errors of two-qubit gates can be mitigated by single-qubit recovery operations. However, this is not a natural assumption in FTQC since what operations are noisy and time-consuming is different from

NISQ architecture. More concretely, even Clifford operations involving only one logical qubit suffer decoding errors.

Here, we show a construction of FTQC architecture that implements QEM with small overheads. The keys are two significant properties of FTQC architecture: logical Pauli operations are error-free and instant by updating the Pauli frame, and a noise map of decoding errors can be assumed as stochastic Pauli noise. Thanks to these properties, we can mitigate all the Clifford operations and Pauli channels only by updating the Pauli frame. Then, error-mitigated Clifford operations and Pauli measurements are available. Because they form a complete basis for mitigating arbitrary errors [12], we can mitigate approximation errors due to Solovay-Kitaev decomposition. Since approximation errors are exactly known in advance, an unbiased estimator free from approximation error can be obtained, which will be explained in Sec. III B 3.

In order to make our QEM procedure to work, accuracy and efficiency of estimation for decoding errors are vital. We will discuss this point in Sec. III C. We show a refined gate set tomography well-suited for our framework which significantly improves estimation of decoding errors. This dramatically saves the time for estimating the noise model, which is negligible compared to the whole computing time.

### 2. Quantum error mitigation for decoding errors

We can express the inverse channel of the non-uniform depolarizing channel Eq. (8) as a linear combination of Pauli operations. Thus, we can express the inverse channel as

$$\begin{aligned} \mathcal{N}_{\text{dec}}^{-1}(\rho) &= \sum_{g \in \{I_L, X_L, Y_L, Z_L\}^{\otimes m}} \eta_g g \rho g^\dagger \\ &= \gamma_{\text{dec}} \sum_{g \in \{I_L, X_L, Y_L, Z_L\}^{\otimes m}} q_g \text{sgn}(\eta_g) g \rho g^\dagger. \end{aligned} \quad (12)$$

Refer to Appendix. B for concrete expression of each coefficient  $\eta_g$ ,  $\gamma_{\text{dec}}$ , and  $q_g$ . Thus we can suppress the errors by applying probabilistic error cancellation only with Pauli operators after decoding processes. The QEM cost for decoding errors in the entire circuit can be expressed as  $\gamma_{\text{dec}}^{\text{tot}} = \prod_{k=1}^{N_{\text{dec}}} \gamma_{\text{dec}}^{(k)}$ , where  $N_{\text{dec}}$  is the number of logical gates, and  $\gamma_{\text{dec}}^{(k)}$  is a QEM cost of the  $k$ -th operation.

Note that probabilistic error cancellation usually applies recovery operations of QEM just after noisy gates [10, 12]; however, because we only perform logical Pauli operations as recovery operations for decoding errors, they can be done only by updating the Pauli frame instead of directly applying it after noisy gates. Finally, the measurement result is post-processed according to the state of the Pauli-frame, the parity corresponding to the applied recovery operations, and the QEM cost. Thus, unlike probabilistic error cancellation for NISQ devices,

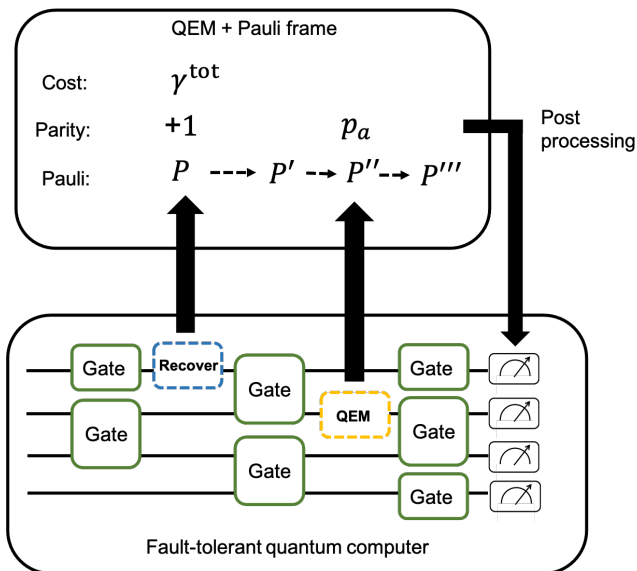


FIG. 2. Schematic figure for Pauli frame incorporating QEM. If a QEM recovery operation is a Pauli operation, it is not directly applied on the quantum computer but the Pauli frame is updated instead. According to generated recovery operations of QEM, the parity is also updated. Here we denote the parity corresponding to the QEM recovery operation as  $p_a$  in the figure. If a QEM recovery operation is not a Pauli operator, it is physically performed. Then measurement outcomes are post-processed depending on the Pauli frame, parity, and QEM cost.

the logical noise due to decoding errors can be mitigated without any noise by recovery operation. The schematic figure is shown in Fig. 2. We remark that the information of the QEM cost and the parity is used only when the final measurement result is obtained; the outcome of a destructive logical Pauli measurement is flipped depending only on the state of the Pauli frame. Strictly saying, whether we can mitigate decoding errors of complex logical operations such as gate teleportation or adaptive Clifford gates only by Pauli frame updates is not trivial. We provide concrete procedure for actual devices and Pauli frames in Appendix. E.

By approximating the QEM cost in the first order of the logical error, we can show

$$\gamma_{\text{dec}} \simeq 1 + 2p_{\text{dec}}. \quad (13)$$

Refer to Appendix. B for details. Under the assumption that the logical error rate is the same for all the logical operations and  $p_{\text{dec}}N_{\text{dec}} = O(1)$  with  $p_{\text{dec}} \rightarrow +0$ , the QEM cost  $\gamma_{\text{dec}}^{\text{tot}}$  for the entire quantum circuit is exactly equal to  $e^{2p_{\text{dec}}N_{\text{dec}}}$  based on the argument in Sec. II A. Thus, by using Eqs. (9) and (10), we obtain

$$\gamma_{\text{dec}} - 1 = 2mC_1 \left( C_2 \frac{p}{p_{\text{th}}} \right)^{(d+1)/2}, \quad (14)$$

which results in the total QEM sampling overhead

$$\Gamma_L^{\text{tot}} = e^{2(\gamma_{\text{dec}}-1)N_{\text{dec}}} = \exp \left( 4mC_1N_{\text{dec}} \left( C_2 \frac{p}{p_{\text{th}}} \right)^{(d+1)/2} \right). \quad (15)$$

Notice that Eq. (15) clearly shows a trade-off relationship between the sampling overhead and the code distance, i.e., the number of physical qubits.

### 3. Quantum error mitigation for approximation errors

Unlike decoding errors due to failure of error correction, we cannot convert approximation errors by Solovay-Kitaev decomposition into stochastic Pauli errors. Nevertheless, we can still apply probabilistic error cancellation with negligible overheads. Denote  $\mathcal{N}_{\text{SK}}(\rho) = \tilde{U}U\rho(\tilde{U}U)^\dagger$ , we invert this approximation error by

$$\begin{aligned} \mathcal{N}_{\text{SK}}^{-1} &= \sum_i \eta_i \mathcal{B}_i^{(L)} \\ &= \gamma_{\text{SK}} \sum_i q_i \text{sgn}(\eta_i) \mathcal{B}_i^{(L)}, \end{aligned} \quad (16)$$

where  $\{\mathcal{B}_i^{(L)}\}$  is recovery operations on logical space. Note that we can represent any map as a linear combination of Clifford operations and Pauli channels [12], and thus we do not need  $T$ -gates for mitigating approximation errors. Recovery operations are randomly chosen and applied just after each single-qubit logical operation if they are not Pauli operations. In the case of Pauli operations, we can again use Pauli frame, and physical operations on quantum computers are not required in a similar vein to QEM for decoding errors. Since a single-qubit logical unitary operation consists of several repetition of Clifford gates and  $T$ -gate teleportation, the insertion of the recovery operation for probabilistic error cancellation negligibly increases the length of quantum circuit. In numerical simulations in the next section, we will verify that QEM costs can be approximated with the following equation:

$$\gamma_{\text{SK}} - 1 = \beta_1 e^{-\beta_2 N_T}, \quad (17)$$

where  $\beta_1$  and  $\beta_2$  are constants dependent on a quantum gate and  $N_T$  is the number of available  $T$ -gates.

The QEM cost due to approximation errors can also be represented as  $\gamma_{\text{SK}}^{\text{tot}} = \prod_{k=1}^{N_{\text{SK}}} \gamma_{\text{SK}}^{(k)}$ , where  $N_{\text{SK}}$  is the total number of recovery operations for mitigating approximation errors in the quantum circuit with the cost  $\gamma_{\text{SK}}^{(k)}$  corresponding to the  $k$ -th recovery operation. By assuming that the cost does not depend on gates, we have the following QEM sampling overhead:

$$\Gamma_{\text{SK}}^{\text{tot}} \simeq \exp(2\beta_1 N_{\text{SK}} e^{-\beta_2 N_T}). \quad (18)$$

This indicates a trade-off relationship between the sampling overhead and the number of available  $T$ -gates.

### C. Effect of estimation errors of the noise map

#### 1. The effect of estimation errors on expectation values

While approximation errors can be exactly known in advance, decoding errors are needed to be characterized. Since logical error probabilities of decoding errors are small, it is unavoidable that characterization contains finite and non-negligible estimation errors. Thus, we need to care about QEM with estimation errors and efficiency of characterization on decoding errors.

Here we discuss how estimation errors result in the performance of QEM. Assume that the actual error model for the  $k$ -th gate  $\mathcal{U}_k$  is a stochastic error represented as  $\mathcal{N}_k = (1 - \varepsilon_k)\mathcal{I} + \varepsilon_k\mathcal{E}_k$ . Here  $\mathcal{E}$  is a trace-preserving and completely positive (TPCP) map describing the noise event. In the FTQC setup, we have  $\varepsilon_k = p_{\text{dec}}^{(k)}$ , where  $p_{\text{dec}}^{(k)}$  is a logical error probability per gate due to decoding failure; however, the argument below can be applied for conventional NISQ scenarios, we continue denoting the error probability as  $\varepsilon_k$ . Given the perfect characterisation of the noise model, we can realise the inverse operation  $\mathcal{N}_k^{-1}$  with probabilistic error cancellation to achieve  $\mathcal{N}_k^{-1}\mathcal{N}_k = \mathcal{I}$ . When we obtain a wrong estimation for the error process  $\mathcal{N}'_k \neq \mathcal{N}_k$ , it leads to  $\mathcal{N}'_k^{-1}\mathcal{N}_k = (1 - \Delta\varepsilon_k)\mathcal{I} + \Delta\varepsilon_k\mathcal{E}'_k$ . Here, we denote  $\Delta\varepsilon_k$  as the effect of model estimation error with  $\mathcal{E}'_k$  being the corresponding TPCP map. Now, the error mitigated state from the entire quantum circuit can be written as

$$\begin{aligned} \rho_{\text{QEM}} &= \prod_{k=1}^{N_G} ((1 - \Delta\varepsilon_k)\mathcal{I} + \Delta\varepsilon_k\mathcal{E}'_k)\mathcal{U}_k(\rho_{\text{in}}) \\ &= \left[ \prod_{k=1}^{N_G} (1 - \Delta\varepsilon_k) \right] \mathcal{U}_{\text{id}}(\rho_{\text{in}}) \\ &\quad + \left[ 1 - \prod_{k=1}^{N_G} (1 - \Delta\varepsilon_k) \right] \mathcal{E}_{\text{tot}}(\rho_{\text{in}}), \end{aligned} \quad (19)$$

where  $\mathcal{U}_{\text{id}} = \prod_{k=1}^{N_G} \mathcal{U}_k$  and  $\mathcal{E}_{\text{tot}}$  is a process which is affected by at least one error event. Now the trace distance of the error mitigated state  $\rho_{\text{QEM}}$  and the ideal state  $\rho_{\text{id}} = \mathcal{U}_{\text{id}}(\rho_{\text{in}})$  can be upper bounded as

$$D(\rho_{\text{QEM}}, \rho_{\text{id}}) = \frac{1}{2} \|\rho_{\text{QEM}} - \rho_{\text{id}}\|_1 \leq 1 - \prod_{k=1}^{N_G} (1 - \Delta\varepsilon_k). \quad (20)$$

Here we used  $\|\alpha_k \rho_k\|_1 \leq \sum_k |\alpha_k| \|\rho_k\|_1 = \sum_k |\alpha_k|$  for quantum states  $\rho_k$  and  $\alpha \in \mathbb{C}$ . Because the difference of the expectation values of the ideal state and the error-mitigated state can be upper bounded for an observable  $M$  as  $\delta M = \text{Tr}[M(\rho_{\text{id}} - \rho_{\text{QEM}})] \leq$

$2\|M\|_1 D(\rho_{\text{id}}, \rho_{\text{QEM}})$  [36, 37], we have

$$\begin{aligned} \delta M &\leq 2\|M\| \left( 1 - \prod_{k=1}^{N_G} (1 - \Delta\varepsilon_k) \right) \\ &\sim 2\|M\| (1 - e^{\Delta\varepsilon N_G}), \end{aligned} \quad (21)$$

where  $\|\cdot\|$  represents an operator norm, we set  $\Delta\varepsilon_k = \Delta\varepsilon$  and assume  $\Delta\varepsilon N_G = O(1)$  for sufficiently large  $N_G$ . Note that this discussion does not include sampling errors; i.e.,  $\delta M$  is the error of the expectation value given infinite samples. Thus, we can see that QEM is beneficial when we can achieve  $\Delta\varepsilon = r\varepsilon$  ( $r < 1$ ) in the case that we have a large number of samples. For example, when  $\varepsilon N_G \ll 1$ , we have  $\delta M \lesssim 2r\|M\|N_G\varepsilon$ , which implies  $r$  times higher accuracy.

#### 2. The efficiency of characterization of decoding errors

As a cause for model estimation errors, when we apply gate set tomography to characterize the noise model for decoding errors, we need to consider the finite statistical error due to insufficiency of the number of samples and state preparation and measurement (SPAM) errors. It has been shown that the effect of SPAM errors can be eliminated at the cost of statistical accuracy in the case of probabilistic error cancellation based on gate set tomography [12], and we show that this method is compatible with QEM with the Pauli frame in Appendix C. We propose a suitable procedure for gate set tomography for our scheme, and the number of measurements  $N_{\text{GST}}$  to characterize the noise model for achieving the estimation error to the level of  $r\varepsilon$  ( $r < 1$ ) is  $N_{\text{GST}} = O(r^{-2}\varepsilon^{-1})$ . Let the time for single-shot computation be  $\tau$ . Then the time per gate can be roughly approximated as  $\tau_{\text{gate}} = \tau/N_G$ , and the time for gate set tomography is estimated as  $\tau_{\text{GST}} = \tau_{\text{gate}}N_{\text{GST}} = O(\tau r^{-2}(\varepsilon N_G)^{-1})$ . This means we need GST whose repetition is in the order of  $O(r^{-2}(\varepsilon N_G)^{-1})$ . Note that in the FTQC scenario,  $\varepsilon N_G$  corresponds to the average number of logical Pauli errors  $p_{\text{dec}}N_{\text{dec}}$ . When we consider a situation where QEM is useful, i.e.,  $\varepsilon N_G = O(1)$  [19], we can conclude that to decrease logical error rate  $p_{\text{dec}}$  to  $rp_{\text{dec}}$  by QEM, we need gate set tomography as pre-computation that takes  $O(r^{-2})$  times longer than a single circuit run of FTQC. Note that when FTQC is used for calculating an expectation value, circuit runs of FTQC are repeated to achieve a required accuracy. Thus, as far as  $r$  is not too small, a time for this pre-computation is expected not to be dominant.

#### 3. Effective increase of code distance by quantum error mitigation under estimation errors

We can regard that QEM effectively increases the code distance. Assume that we perform gate set tomography with  $O(r^{-2})$  times more repetitions and effectively

achieve  $r$  times smaller logical error rate  $p_{\text{eff}} = rp_{\text{dec}}$ . Since the logical error rate is roughly approximated with the code distance as  $p_{\text{dec}}(d) = p(p/p_{\text{th}})^{(d-1)/2}$ , QEM effectively achieves larger code distance  $d'$  where  $p_{\text{eff}} = p_{\text{dec}}(d')$  without increasing the number of physical qubits. The effective increase of the code distance via QEM can be derived as

$$d' - d = 2 \frac{\ln r}{\ln\left(\frac{p}{p_{\text{th}}}\right)}. \quad (22)$$

Therefore, by setting  $r = (p/p_{\text{th}})^x$ , we can effectively increase the code distance by  $2x$ . Note that as discussed in the previous sections, we need to have  $\exp(O(N_{\text{dec}}p_{\text{dec}})) = \exp(O(1))$  times more repetitions to achieve the same precision as the error-free case and the time for error characterization which scales as  $O(r^{-2}\tau)$ . It is worth noting that we can increase the number of available logical qubits via QEM. When we are allowed to use a fixed number of physical qubits, the decrease of the code distance indicates that we can allocate more logical qubits; therefore, we can convert the code distance to the number of logical qubits.

#### IV. NUMERICAL ANALYSIS

In this section, we numerically evaluate how error mitigation can suppress the required qubit overhead in FTQC. First, we numerically investigate the efficiency of QEM for each factor of errors introduced in Sec. III. See Appendix. G for detailed settings and definitions of numerical analysis.

##### A. Quantum error mitigation for decoding errors

###### 1. Cost analysis

First, we evaluate the performance of QEM for decoding errors during logical operations, where we assume FTQC with surface codes and lattice surgery. For details about surface codes, see Appendix. D. For simplicity, we assume a single-qubit depolarizing noise model occurs on each data and measurement qubits at the beginning of each cycle, which corresponds to a phenomenological noise model [38, 39]. To determine a failure probability of decoding with faulty syndrome-measurement cycles, we assume perfect syndrome measurements at the 0-th and  $d$ -th cycles. Then we check whether logical Pauli errors occurred during  $d$  cycles. Recovery operations are estimated from syndrome values with minimum-weight perfect matching algorithm [40, 41]. We evaluate logical error probabilities of Pauli- $X, Y, Z$  and compute a QEM cost for  $d$  cycles according to Eq. (B5). Despite the assumption of perfect syndrome measurements of 0-th and  $d$ -th cycle, we expect that numerical results become asymptotically equivalent to those without the assumption when  $d$  is sufficiently large.

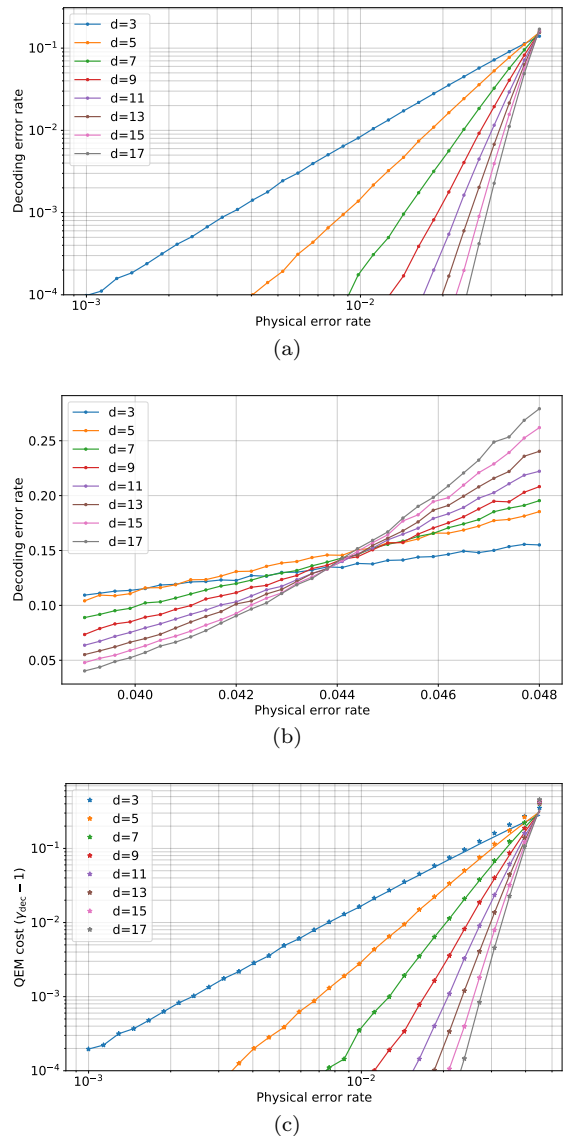


FIG. 3. Logical error probabilities and QEM costs for  $d$ -cycle syndrome measurements are plotted according to physical error rates at several code distances. (a) Logical error probabilities as a function of physical error rate. (b) The same figure zoomed around a threshold value. (c) QEM costs for  $d$ -cycle idling operations. The first order approximations from Eq. (13) are shown as solid lines.

Logical error probabilities of Pauli- $X, Y, Z$  of a single logical qubit for several code distances are calculated, and the sum of their probabilities are plotted according to physical error rates in Fig. 3(a). A logical error probability is exponentially reduced according to the code distance when physical error probability  $p$  is smaller than a threshold value. A behavior of logical error probabilities around a threshold value is plotted in Fig. 3(b), which is around  $p_{\text{th}} = 0.044$ .

We compute QEM costs for decoding errors  $\gamma_{\text{dec}}$  corresponding to  $d$  cycles and different code distances, and

compared them with the first order approximation shown in Eq. (13). Numerical results are plotted in Fig. 3(c). In this figure, solid lines correspond to an approximation of QEM costs in Eq. (13). We see that QEM costs also decay exponentially depending on the code distances and show a threshold behavior like logical error probabilities. They coincide well when the physical error rate is sufficiently small.

## 2. Performance analysis

We demonstrate the performance of QEM for decoding errors in large-scale quantum circuits with a 100-qubit logical random Clifford circuit with 100 layers. We remark that since a linear combination of Clifford operations can represent arbitrary quantum operations, it is sufficient to demonstrate the performance of QEM for Clifford operations [17]. In each layer, randomly generated single-qubit Clifford gates are simultaneously applied, and then 50 CNOT gates are applied to randomly paired two qubits. Owing to an efficient algorithm of stabilizer circuits [29, 42], we can simulate these protocols efficiently. As an observable, we choose a Pauli operator whose measurement outcome is always unity for the final state vector if there are no physical errors, i.e., the final state is a +1 eigenstate of the chosen observable. In numerical simulations, we assume a non-uniform single-qubit depolarizing logical error in the form of Eq. (8) for each layer. Logical error probabilities of depolarizing channels are determined according to the numerical results of the last section. In this simulation, we choose  $p = 0.01$ , and logical error probabilities are obtained with extrapolation. Logical error probabilities that we estimate are summarized in TABLE I. Without QEM, the

code distance $d$	$p_{X_L}, p_{Z_L}$	$p_{Y_L}$
5	$1.80 \times 10^{-4}$	$1.96 \times 10^{-6}$
7	$1.39 \times 10^{-5}$	$4.11 \times 10^{-8}$
9	$1.08 \times 10^{-6}$	$8.64 \times 10^{-10}$
11	$8.35 \times 10^{-8}$	$1.81 \times 10^{-11}$

TABLE I. Estimated logical error probabilities for code distances with  $p = 0.01$  and  $p_{\text{th}} \sim 0.044$ .

final state converges to a highly mixed state due to physical errors. Thus, it is expected that expectation values decay to zero. By employing QEM, they are taken back to unity, sacrificing statistical accuracy and requiring a greater number of experiments accordingly.

Note that while a required number of cycles for Clifford operations scales linearly with the code distance, the actual number of cycles and logical error probability per logical gate are dependent on a Clifford operation. In particular, logical CNOT gates with lattice surgery may induce correlated logical Pauli errors on multiple logical qubits. Nevertheless, we use a simplified error model

since we expect this evaluation captures the basic properties of QEM performance.

We numerically perform a series of  $10^4$  experiments, each of which computes an expectation values with  $10^4$  single-shot measurements. The results are shown in Fig. 4(a), and detailed data around ideal expectation value is shown in Fig. 4(b). The mean value of  $10^4$  samples for each logical error probabilities are shown in Fig. 4(c) with its standard deviation as an error bar. We see there is a large bias in an expectation value without QEM. On the other hand, there is no bias when QEM technique is employed, while its standard deviation is amplified. A standard deviation of expectation values with  $d = 5$  is 14.2, and thus not visible in the histogram because it is too large. The mean number of Pauli errors in the whole quantum circuit is 3.6 in  $d = 5$  and 0.28 in  $d = 7$ . Thus, as explained in Sec. II A, QEM is typically useful when the number of Pauli errors in the circuit is  $O(1)$ . We see that QEM technique is effective in large-scale quantum computing, and enables us to increase effective code distance.

## B. Quantum error mitigation for approximation errors

### 1. Cost analysis

Here, we study the performance of QEM under Solovay-Kitaev decomposition. Since the actual QEM cost  $\gamma_{\text{SK}}$  depends on a target unitary operator, we draw a sample of unitary operation  $U$  from Haar-measure random distribution  $\mu_{\text{H}}$ . Then, we decompose a unitary gate in the form of  $U = R_Z(\theta_1)\sqrt{X}R_Z(\theta_2)\sqrt{X}R_Z(\theta_3)$ , where  $\sqrt{X} = HSH$  is a Clifford operation. We use an improved Solovay-Kitaev algorithm shown in Ref. [35]. This algorithm enables us to approximate an arbitrary Pauli- $Z$  rotation  $R_Z(\theta) = \exp(i\frac{\theta}{2}Z)$  with an operator  $\tilde{U}$  which is described as a sequence of Clifford operations and  $T$ -gates. We set the maximum count of  $T$ -gate for each decomposition for three Pauli- $Z$  rotations to check a trade-off relation between a  $T$ -gate count and an approximation accuracy. A histogram of errors evaluated with operator norm  $\|U - \tilde{U}\|$  is shown in Fig. 5(a). As expected, an exponential decrease of approximation errors is observed.

Then, we calculate QEM costs by using Eq. (16). A histogram for QEM costs  $\gamma_{\text{SK}}$  is shown in Fig. 5(b). We show QEM costs versus the number of allowed  $T$ -gates in Fig. 5(c). We can see that  $\gamma_{\text{SK}} - 1$  exponentially reduces according to the number of  $T$ -gates, and its variance also decreases exponentially. We fit the QEM cost  $\gamma_{\text{SK}}$  with Eq. (17), and obtain  $\beta_1 = 3.9(5)$  and  $\beta_2 = 0.072(1)$ .

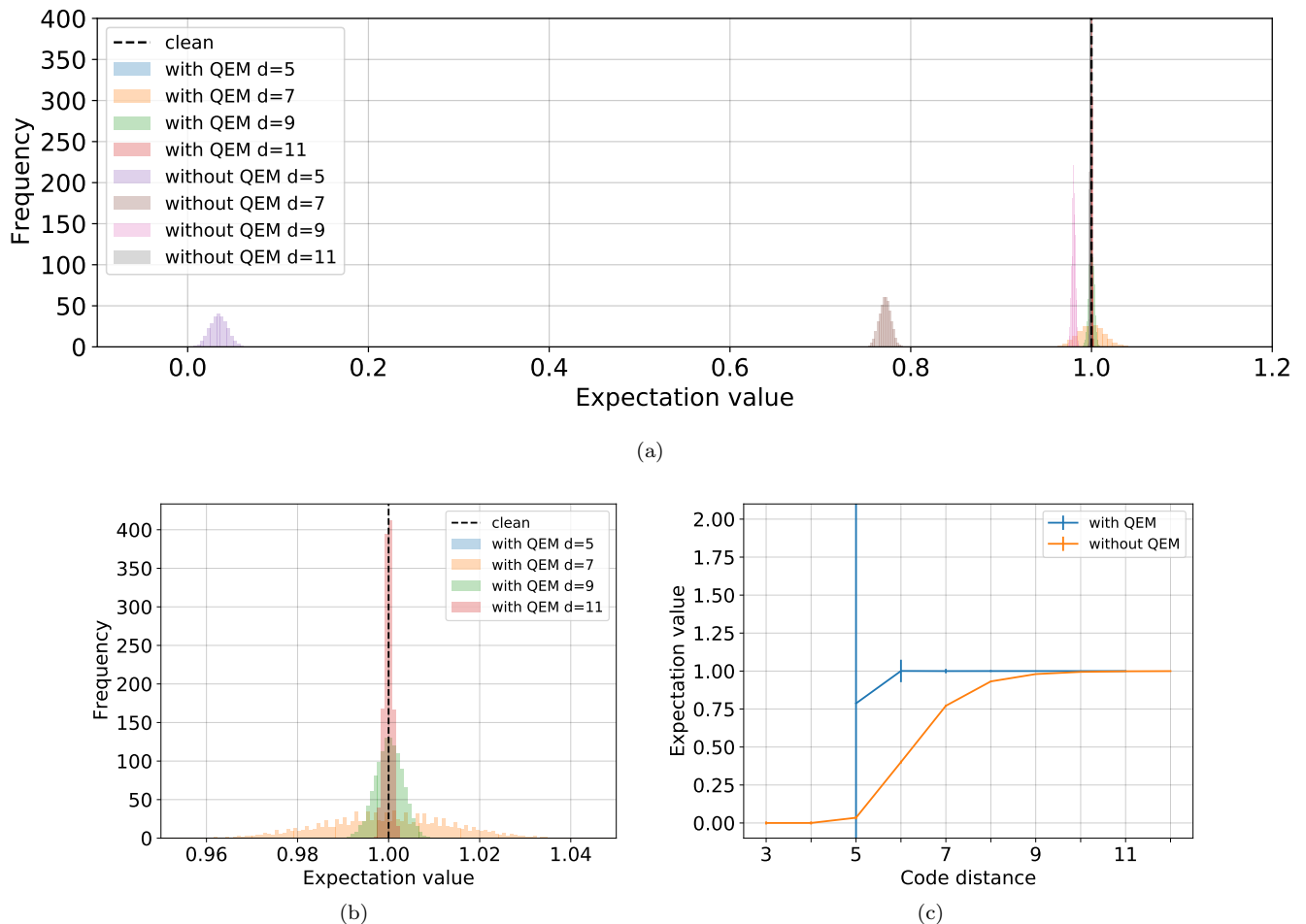


FIG. 4. (a) A histogram for expectation values for 100-qubit random Clifford circuits. (b) A histogram for expectation values with QEM for 100-qubit random Clifford circuits. (c) Sample averages and standard deviation of 100-qubit random Clifford circuits are plotted as a function of code distances.

## 2. Performance analysis

Next, we evaluate the performance of QEM for approximation errors due to Solovay-Kitaev decomposition via simulation of a SWAP test circuit with 7 qubits. A SWAP test circuit evaluates the overlap of two input states  $\rho$  and  $\sigma$  as  $\text{Tr}[\rho\sigma]$  by measuring an ancilla qubits [43]. We set one of the input states to the ideal state and the other to the state affected by approximation errors. A schematic is shown in Fig. 6.

The ideal state is generated by random quantum circuits which consist of three layers. In each layer, random single-qubit unitary operations are simultaneously applied, then a CNOT gate acts on randomly chosen two qubits. The same random quantum circuit is applied to the approximated state by employing Solovay-Kitaev decomposition to each single-qubit rotation. If there are no approximation errors, since the input states are the same, we necessarily obtain +1 as measurement outcomes hence the expectation value is also +1 for the Pauli-Z operator of the ancilla qubit. On the other hand, an expecta-

tion value becomes smaller than unity when the inner product is reduced due to approximation errors. Since approximation errors cannot be treated in a framework of stabilizer simulation, we simulate quantum circuits by directly updating the state vector after each gate.

We also numerically perform a series of  $10^4$  experiments and compute expectation values from  $10^4$  single-shot measurements. The number of allowed  $T$ -gates in each Solovay-Kitaev decomposition for single-qubit unitary operations is chosen from 24 to 60. The results are shown in Fig. 4(a), and detailed data around ideal expectation value is shown in Fig. 4(b). The mean value of  $10^4$  samples for each logical error probabilities are shown in Fig. 4(c) with its standard deviation as an error bar. Note that standard deviation with 21  $T$ -gates is 4.65. We see that our QEM technique successfully removes a bias of the expectation value in noisy cases. Compared to the QEM costs for decoding errors, we obtain larger QEM costs. This is consistent with the results reported in Ref. [12] that QEM costs for unitary errors tend to be larger than stochastic errors.

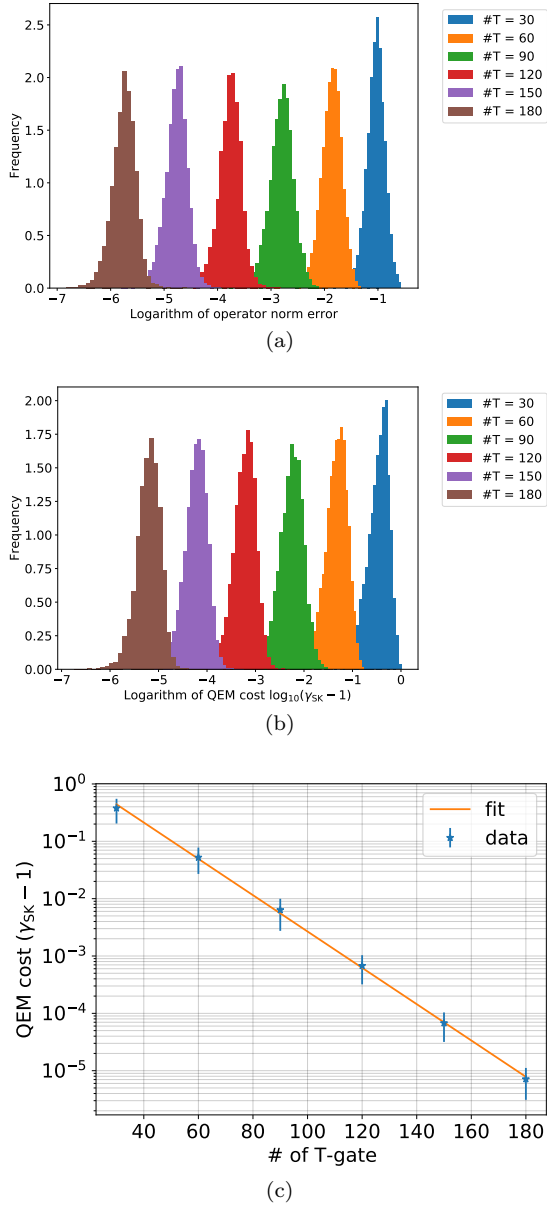


FIG. 5. Approximation errors and QEM costs of improved Solovay-Kitaev method are calculated for Haar-random unitary operations. Each color corresponds to the maximum count of  $T$ -gate. (a) A histogram of approximation errors due to Solovay-Kitaev decomposition. (b) A histogram for QEM costs. (c) A histogram of QEM costs for approximation errors as a function of the number of allowed  $T$ -gates.

This problem may be relaxed by performing several Solovay-Kitaev decomposition with the same accuracy, constructing randomizing approximation errors, and removing a coherent component of noise. Note that with sufficiently large sample size, our QEM technique increases an effective number of  $T$ -gates by inserting additional Clifford gates and Pauli channels and repetitive sampling, which can be achieved with negligible additional hardware requirements.

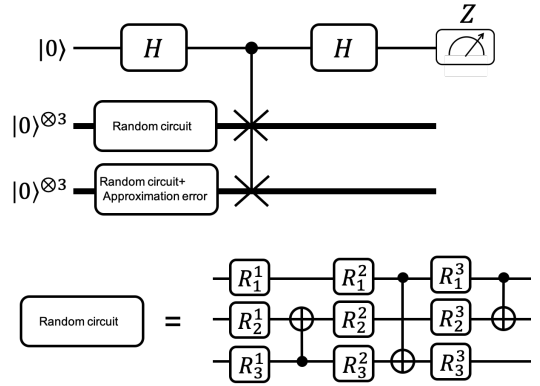


FIG. 6. Schematic figure for a 7-qubit SWAP test circuit we simulate. We calculate the overlap of randomly generated states and the approximation of the generated state via Solovay-Kitaev algorithm. The random circuit is constructed by three layers, each of which composes of random single-qubit rotation gates and CNOT gates to randomly chosen two qubits.

### C. Quantum error mitigation with estimation errors

Probabilistic error cancellation assumes noise maps to cancel are known in advance. While we can know an approximation error of Solovay-Kitaev decomposition within a numerical precision, it is hard to exactly characterize noise maps of decoding errors due to several reasons because GST suffers from finite sampling as discussed in Sec. III C. In this section, we numerically evaluate the performance of our framework under finite estimation errors.

For the benchmarks, we choose the same quantum circuit, noise model, and observable as the Sec. IV A 2. We evaluate an expectation value under a 100-qubit noisy Clifford circuit that becomes unity if there is no noise. Non-uniform depolarizing channel where Pauli- $X, Y, Z$  occurs with probabilities  $(p_x, p_y, p_z)$  is inserted after each gate. We use the probabilities obtained from the simulation of surface codes shown in Table I. The different point from the previous simulations is that these probabilities are over- or under-estimated as  $((1+r)p_x, (1+r)p_y, (1+r)p_z)$  ( $r > -1$ ) in probabilistic error cancellation. Here,  $r = 0$  corresponds to exact characterization and perfect error mitigation, and  $r = -1$  corresponds to FTQC without error mitigation. According to the discussion in Sec. III C, we expect a distribution such that its mean value is the same as that of the simulation under mitigated noise model ( $|r\rangle p_x, |r\rangle p_y, |r\rangle p_z$ ) and its variance is approximately  $\Gamma$  where  $\Gamma$  is the overhead of QEM determined by estimated noise model  $((1+r)p_x, (1+r)p_y, (1+r)p_z)$ . The histogram under finite estimation errors parametrized by  $r$  for  $d = 7$  and  $d = 9$  are plotted in Fig. 8(a), and its mean values and standard deviations are plotted as a function of  $r$  in Fig. 8(b). We observe that the residual bias increases exponentially ac-

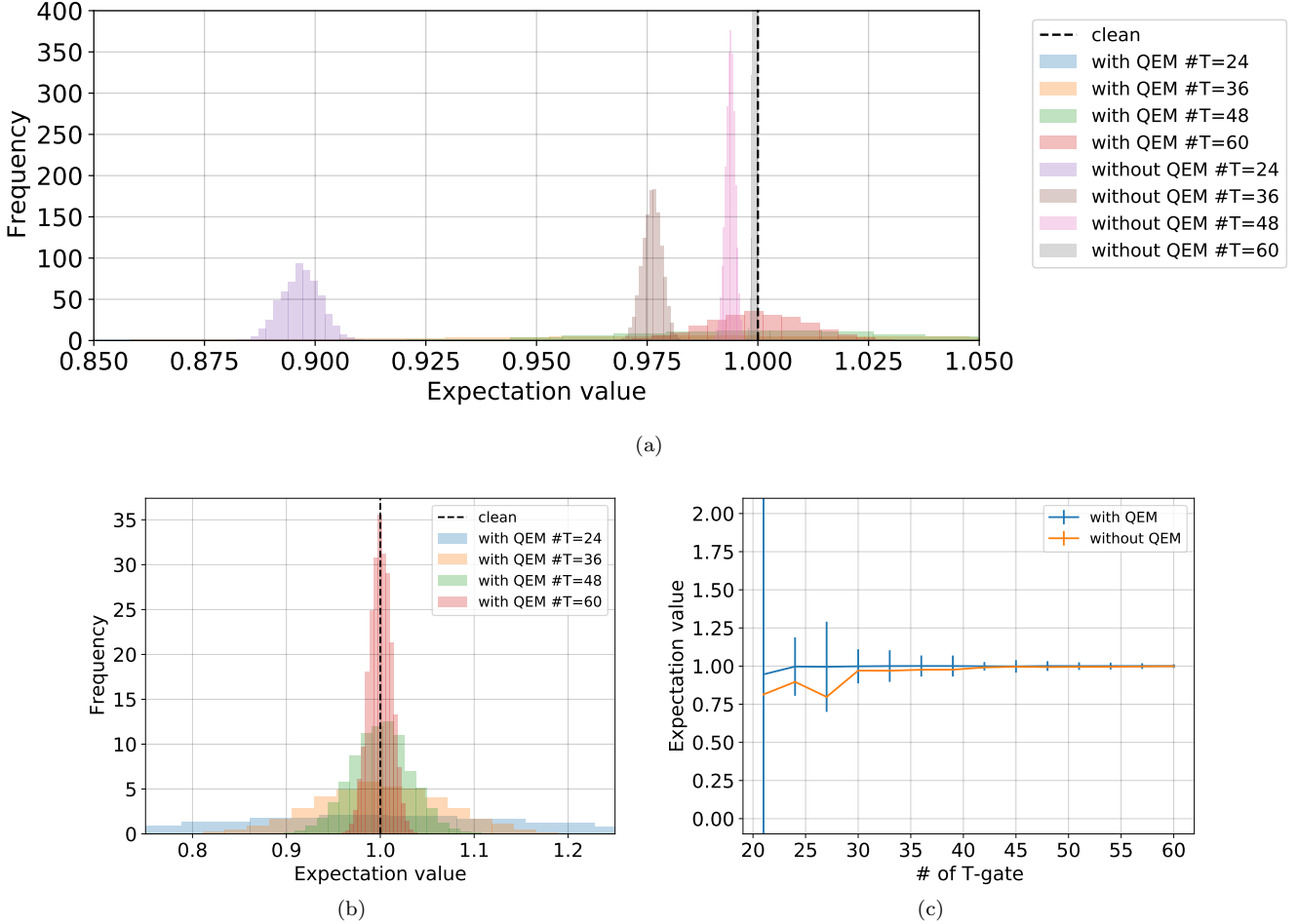


FIG. 7. A histogram for expectation values of SWAP test with approximation errors. (a) A histogram of expectation values. (b) The same figure zoomed around an ideal expectation value. (c) Sample averages and standard deviation as a function of the allowed number of  $T$ -gates.

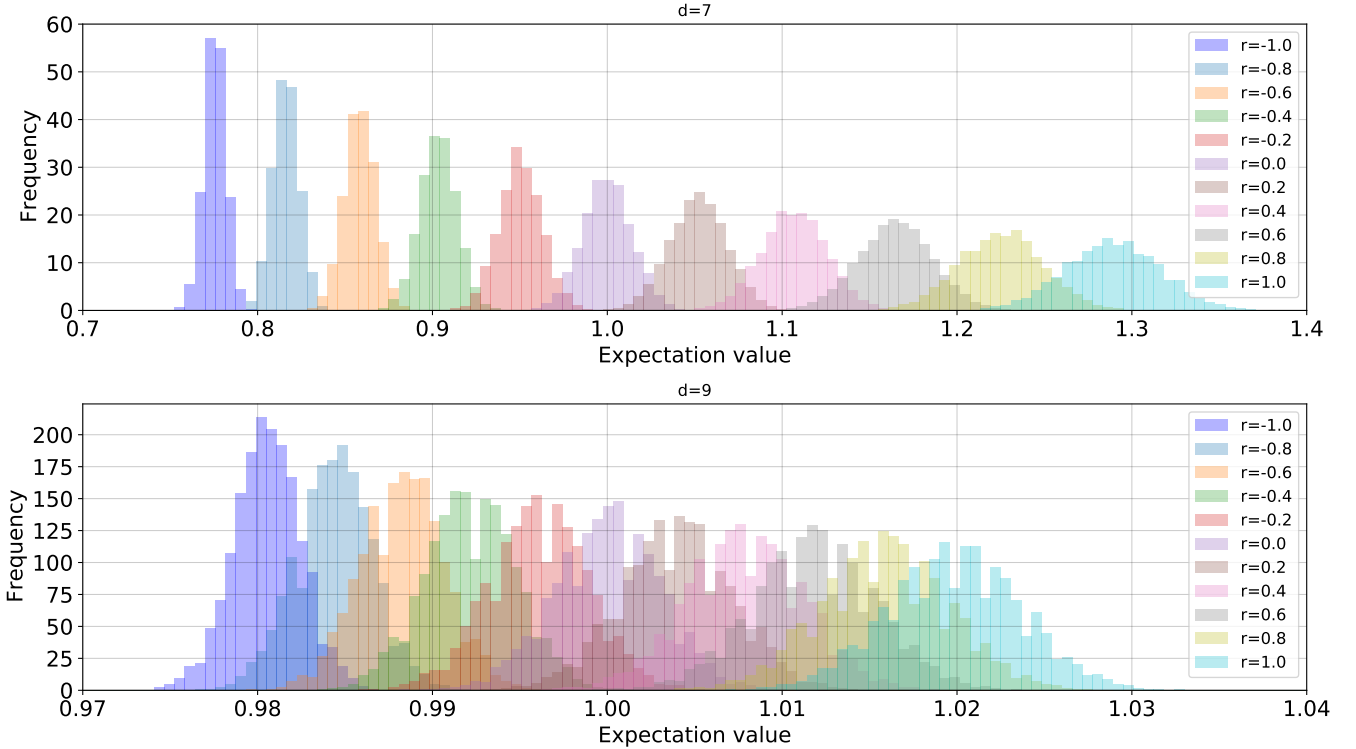
according to  $|r|$ , which agrees with the results discussed in Sec. III C. With an infinite samples, QEM is always beneficial when  $|r| < 1$ . Comparing the case where under-estimation  $r < 0$  and over-estimation  $r > 0$  with the same absolute value  $|r|$ , over-estimation ( $r > 0$ ) has larger variance than under-estimation ( $r < 0$ ) while there is similar amount of bias in expectation values. Since QEM prefers under-estimation to over-estimation, characterization methods with weighted penalty may be useful for further improvement of QEM.

## V. DISCUSSION

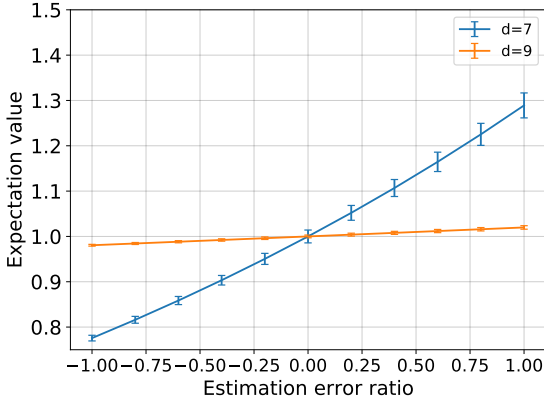
In this work, we show an approach to effectively decrease errors in FTQC by performing QEM in the logical space. In the case of decoding errors, owing to the Pauli frame, we can perform QEM without implementing any physical operations if decoding errors are stochastic Pauli maps, while QEM induces additional errors when we implement it physically on general quantum circuits. For

approximation errors by Solovay-Kitaev decomposition, we cannot always use the Pauli frame because not only Pauli operations but also Clifford operations and Pauli measurements are employed for QEM in general. Since Clifford operations can be efficiently performed in FTQC and the number of decoding processes for error correction is much larger than the gate count in Solovay-Kitaev algorithms, this overhead is negligible. We also verify the trade-off between costs of QEM and the code distance and the number of  $T$ -gates. Furthermore, we estimated the sampling cost of gate set tomography to obtain the decoding noise map to a required accuracy, and we clarified that our approach enables quantum computing corresponding to more than the achievable code distance.

One of the promising applications of our method is Hamiltonian simulation of quantum many-body dynamics. There are algorithmic errors in Trotter decomposition [44] and in recently proposed methods such as Taylor series [45] and quantum signal processing [46, 47]. As these errors involve the entire quantum computer, it is hard to estimate the probabilistic cancellation map. In



(a)



(b)

FIG. 8. A histogram for expectation values with estimation errors. (a) A histogram of expectation values. (b) Sample averages and standard deviation as a function of estimation accuracy.

Refs. [48, 49], it is shown that such algorithmic errors can be mitigated by employing extrapolation. Since algorithmic errors can be controlled by changing simulation accuracy, this technique can also be naturally applied in the FTQC scenario. Thus dominant errors in FTQC can be compensated via QEM.

The first generation of FTQC may not be sufficiently large for naively solving large and useful problems. While the architecture of distributed quantum computing is the most straightforward approach to increase the total number of qubits, it requires interconnections between quan-

tum nodes, which induces additional overheads for entanglement distillation. Thus, we sometimes cannot use sufficient code distances for creating logical qubits. In this context, techniques developed in NISQ era [50, 51] for solving larger problems with small NISQ computers may also be useful in the middle-term FTQC. Our work is the first proposal that makes the best of a technique tailored for NISQ devices in the context of FTQC.

Finally, we discuss the difference between our scheme and a similar work that combines QEM with quantum error correction proposed by McClean *et al.* [52]. Their

method considers implementing quantum error correction for NISQ devices via classical post-processing in the case that experimentalists cannot implement stabilizer measurements due to limited connectivity and large error rates of NISQ devices. Although their method enables the projection of the state to the code space via quantum subspace expansion [53], logical errors cannot be fully eliminated. On the other hand, our scheme assumes FTQC can be performed but the number of qubits and  $T$ -gates cannot be increased infinitely. The remarkable advantage of our method is that we can fully eliminate the decoding errors and approximation errors with a greater number of measurements with negligible hardware overhead, given the complete characterization of the noise model.

### ACKNOWLEDGEMENT

This work is supported by PRESTO, JST, Grant No. JPMJPR1916; ERATO, JST, Grant No. JPMJER1601; CREST, JST, Grant No. JPMJCR1771; MEXT Q-LEAP Grant No. JPMXS0120319794 and JPMXS0118068682. Y.S. would like to thank Takatori Sugiyama for a fruitful discussion on gate set tomography. S.E acknowledges useful discussions with Zhenyu Cai and Xiao Yuan.

### Appendix A: Pauli transfer matrix

Any quantum map can be represented as a matrix called Pauli transfer matrix (PTM). Suppose a quantum process  $\mathcal{E}$  for  $n$ -qubit, which maps an  $n$ -qubit density matrix to another density matrix. We denote a set of  $n$ -qubit Pauli operators as  $\mathcal{P}^{(n)} = \{I, X, Y, Z\}^{\otimes n}$ . A set of  $n$ -qubit Pauli operators are a basis of  $4^n \times 4^n$  matrices and its elements are mutually orthonormal as  $\frac{1}{d} \text{Tr}[P_i P_j] = \delta_{ij}$  for  $d = 2^n$ . The PTM representation of a process  $\mathcal{E}$  is defined with the Pauli basis as follows:

$$\mathcal{M}(\mathcal{E})_{ij} = \frac{1}{d} \text{Tr}[P_j \mathcal{E}(P_i)], \quad (\text{A1})$$

where  $P_i$  is the  $i$ -th element of  $\mathcal{P}^{(n)}$ . Note that since any physical process maps self-adjoint operator to self-adjoint one, all the elements of Pauli transfer matrix are a real value. A density matrix can also be represented as a column vector with the Pauli basis:

$$|\rho\rangle\rangle_i = \text{Tr}[P_i \rho]. \quad (\text{A2})$$

Note that an element of vector corresponding to  $P_i = I$  is the trace of  $\rho$ . A measurement of observable  $O$  can be mapped to a row vector

$$\langle\langle O|_j = \frac{1}{d} \text{Tr}[O P_j]. \quad (\text{A3})$$

Note that PTM representation satisfies

$$\text{Tr}[O \mathcal{E}(\rho)] = \langle\langle O | \mathcal{M}(\mathcal{E}) | \rho \rangle\rangle. \quad (\text{A4})$$

There are several important properties of Pauli transfer matrix representation. Denoting a composite map  $\mathcal{E} = \mathcal{E}_A \circ \mathcal{E}_B$ , the PTM representation is given as  $\mathcal{M}(\mathcal{E}_B \circ \mathcal{E}_A) = \mathcal{M}(\mathcal{E}_B) \mathcal{M}(\mathcal{E}_A)$ . Due to linearity of the PTM representation, for a map  $\mathcal{E}' : \rho \mapsto \sum_k q_k \mathcal{E}_k(\rho)$  we have  $\mathcal{M}(\mathcal{E}') = \sum_k q_k \mathcal{M}(\mathcal{E}_k)$ . If there is no confusion, we simply represent the Pauli transfer matrix  $\mathcal{M}(\mathcal{E})$  as  $\mathcal{E}$ .

### Appendix B: Coefficients for quasi-probability decomposition

To perform probabilistic error cancellation for an arbitrary  $m$ -qubit noise map  $\mathcal{N}$ , we need to decompose the inverse of noise map  $\mathcal{N}^{-1}$  as a linear combination of physical quantum processes. According to Ref. [12], any TPCP-map can be represented as a linear combination of Clifford operations and Pauli channels. This is because a set of Pauli transfer matrices of  $m$ -qubit Clifford operations and Pauli channels forms a basis of  $m$ -qubit Pauli transfer matrices. We introduce the following 16 operators:

$$\mathcal{B} = \left\{ I, \sigma_j, \frac{I + i\sigma_j}{\sqrt{2}}, \frac{I + \sigma_j}{2}, \frac{\sigma_j + \sigma_{j+1}}{\sqrt{2}}, \frac{\sigma_j + i\sigma_{j+1}}{2} \right\}, \quad (\text{B1})$$

where  $j \in \{1, 2, 3\}$ ,  $(\sigma_1, \sigma_2, \sigma_3) = (X, Y, Z)$  and  $\sigma_4 = \sigma_1$ . The Pauli transfer matrices of  $\mathcal{B}^{\otimes m}$  comprise a complete basis of  $n$ -qubit Pauli transfer matrices, i.e., any quantum map can be represented as a linear combination of Clifford operations and Pauli channels. Since the application of non-Clifford operations increases requires complex processes such as magic state injection, distillation, and teleportation, this property is vital to perform probabilistic error cancellation for an arbitrary noise map on FTQC.

Specifically, when noise is modeled as stochastic Pauli errors, we can cancel it only with Pauli operations. This is because a set of Pauli transfer matrices of Pauli operations forms a basis of diagonal  $n$ -qubit Pauli transfer matrices. Since we can perform logical Pauli operations only by updating a Pauli frame, which is a classical memory, in FTQC, we can cancel stochastic logical Pauli noise without acting on an actual quantum device. Suppose that the noise model is described by a Pauli transfer matrix acting on  $m$  qubits:

$$\mathcal{N}_{\text{Pauli}} = (1 - p_{\text{err}}) \mathcal{I} + \sum_{g \neq I^{\otimes m}} p_g \mathcal{P}_g, \quad (\text{B2})$$

where  $\mathcal{I}$  is an identity map,  $\mathcal{P}_g$  is the Pauli transfer matrix of Pauli operator  $g$ ,  $p_g$  ( $g \in \{I, X, Y, Z\}^{\otimes m}$ ) is a probability where Pauli error  $g$  occurs, and  $p_{\text{err}} = \sum_{g \neq I^{\otimes m}} p_g$ . This noise can be canceled with the fol-

lowing map:

$$\mathcal{N}_{\text{Pauli}}^{-1} = \sum_g \eta_g \mathcal{P}_g, \quad (\text{B3})$$

where

$$\eta_g = 4^{-n} \sum_{g'} \frac{c(g, g')}{\sum_{g''} p_{g''} c(g', g'')}. \quad (\text{B4})$$

Note that  $c(g, g')$  is a function for two Pauli operators such that  $c(g, g') = 1$  if  $gg' = g'g$  and  $c(g, g') = -1$  otherwise. In the case of a single-qubit Pauli noise, coefficients and QEM cost  $\gamma_Q$  can be explicitly given as follows.

$$\begin{aligned} \eta_I &= \frac{1}{4} \left( 1 + \frac{1}{1-2(p_Y+p_Z)} + \frac{1}{1-2(p_Z+p_X)} + \frac{1}{1-2(p_X+p_Y)} \right) \\ \eta_X &= \frac{1}{4} \left( 1 + \frac{1}{1-2(p_Y+p_Z)} - \frac{1}{1-2(p_Z+p_X)} - \frac{1}{1-2(p_X+p_Y)} \right) \\ \eta_Y &= \frac{1}{4} \left( 1 - \frac{1}{1-2(p_Y+p_Z)} + \frac{1}{1-2(p_Z+p_X)} - \frac{1}{1-2(p_X+p_Y)} \right) \\ \eta_Z &= \frac{1}{4} \left( 1 - \frac{1}{1-2(p_Y+p_Z)} - \frac{1}{1-2(p_Z+p_X)} + \frac{1}{1-2(p_X+p_Y)} \right) \\ \gamma_Q &= \sum_{g \in \{I, X, Y, Z\}} |\eta_g| = \frac{1}{2} \left( -1 + \frac{1}{1-2(p_Y+p_Z)} + \frac{1}{1-2(p_Z+p_X)} + \frac{1}{1-2(p_X+p_Y)} \right) \end{aligned} \quad (\text{B5})$$

Next, we show that the first-order approximation of a QEM cost for stochastic Pauli noise is Eq. (13). Consider an unphysical map as follows:

$$\mathcal{N}'_{\text{Pauli}} \equiv (1 + p_{\text{err}}) \mathcal{I} - \sum_{g \neq I} p_g \mathcal{P}_g, \quad (\text{B6})$$

and we can easily show

$$\|\mathcal{N}'_{\text{Pauli}} \mathcal{N}_{\text{Pauli}} - \mathcal{I}\| \leq 4p_{\text{err}}^2, \quad (\text{B7})$$

where  $\|\cdot\|$  denotes an operator norm for Pauli transfer matrix. Then we can see that  $\mathcal{N}_{\text{Pauli}}$  is the approximation of the inverse map  $\mathcal{N}'_{\text{Pauli}}^{-1}$  up to the first order, and we have  $\mathcal{N}'_{\text{Pauli}} = \mathcal{N}_{\text{Pauli}}^{-1} + O(p_{\text{err}}^2)$ . Then the QEM cost is approximated as

$$\gamma_Q \approx p_{\text{err}} + \sum_g p_g = 1 + 2p_{\text{err}} \quad (\text{B8})$$

when  $p_{\text{err}} \ll 1$ .

### Appendix C: Probabilistic error cancellation with gate set tomography

In this section, we explain how probabilistic error cancellation can be implemented based on the result of gate set tomography. Furthermore, we also show this method is compatible with the Pauli frame.

#### 1. Gate set tomography

Suppose that we aim to characterize gate set  $\{\mathcal{G}_1, \mathcal{G}_2, \dots, \mathcal{G}_{N_s}\}$ , which involves at most  $N$  qubits. To implement gate set tomography, we measure

$$\tilde{\mathcal{G}}_{ij} = \langle\langle O_i | \mathcal{G} | \rho_j \rangle\rangle, \quad (\text{C1})$$

where  $\mathcal{G}$  is one of gates in the gate set and  $\langle\langle O_i |$  and  $|\rho_j\rangle\rangle$  are linearly independent  $4^N$  observables and states. Note that they are generally noisy since there exist state preparation and measurement (SPAM) errors. Let  $O_i^0$  and  $\rho_j^0$  be error-free observables and states. Here, we set  $O_i^{(0)} \in \{I, X, Y, Z\}^{\otimes N}$  and  $\rho_j^{(0)} \in \{|0\rangle, |1\rangle, |+\rangle, |+_y\rangle\}^{\otimes N}$  with  $|+\rangle = \frac{1}{\sqrt{2}}(|0\rangle + |1\rangle)$  and  $|+_y\rangle = \frac{1}{\sqrt{2}}(|0\rangle + i|1\rangle)$ . Note that  $\langle\langle I |$  corresponds to a trivial measurement whose outcome is always unity. By inserting the identity operator  $\mathcal{I} = \sum_k |O_k^{(0)}\rangle\rangle \langle\langle O_k^{(0)}|$ , we obtain

$$\tilde{\mathcal{G}}_{ij} = \sum_{kk'} A_{ik}^{(\text{out})} \mathcal{G}_{kk'} A_{k'j}^{(\text{in})}, \quad (\text{C2})$$

where  $A_{ik}^{(\text{out})} = \langle\langle O_i | O_k^{(0)} \rangle\rangle$ ,  $A_{k'j}^{(\text{in})} = \langle\langle O_{k'}^{(0)} | \rho_j \rangle\rangle$ , and  $\mathcal{G}_{kk'} = \langle\langle O_k^{(0)} | \mathcal{G} | O_{k'}^{(0)} \rangle\rangle$ . Thus we have

$$\tilde{\mathcal{G}} = A^{(\text{out})} \mathcal{G} A^{(\text{in})}. \quad (\text{C3})$$

It is noteworthy that  $A^{(\text{out})}$  and  $A^{(\text{in})}$  are affected by measurement errors and state preparation errors, which

cannot be experimentally measured because they cannot be separated from each other.

In addition, we replace  $\mathcal{G}$  with the identity operation to obtain

$$g = A^{(\text{out})}A^{(\text{in})}. \quad (\text{C4})$$

In a typical scenario of gate set tomography, the estimation of the process is represented as

$$\begin{aligned} \mathcal{G}^{\text{est}} &= Bg^{-1}\tilde{\mathcal{G}}B^{-1} \\ &= BA^{(\text{in})-1}\mathcal{G}A^{(\text{in})}B^{-1} \end{aligned} \quad (\text{C5})$$

with  $B$  being an invertible matrix we can arbitrarily choose. Denoting the error-free  $A^{(\text{in})}$  matrix as  $A^{(\text{in})(0)}$ , one feasible choice is to set  $B = A^{(\text{in})(0)}$  when the initialization error is small. We also estimate the initial state and the measurement as follows:

$$\begin{aligned} |\rho_j^{\text{est}}\rangle\rangle &= B_{\bullet,j} = BA^{(\text{in})-1}|\rho_j\rangle\rangle \\ \langle\langle O_i^{\text{est}}| &= (gB^{-1})_{i,\bullet} = \langle\langle O_i|A^{(\text{in})}B^{-1}, \end{aligned} \quad (\text{C6})$$

which can be computed from the  $B$  matrix and  $g$  matrix. Now, by implementing the same procedure for  $\mathcal{G}_k$  ( $k = 1, 2, \dots, N_s$ ), assuming the identical SPAM errors for each experiment, we estimate  $\mathcal{G}_k^{\text{est}} = BA^{(\text{in})-1}\mathcal{G}_kA^{(\text{in})}B^{-1}$ . Although estimated gate set, initial states and measurements may differ from true ones  $\{|\rho_j\rangle\rangle, \langle\langle O_i|\mathcal{G}_k\}$  due to SPAM errors, they give the correct expectation value for a sequence of gate set as

$$\langle\langle O_i^{\text{est}}| \prod_k \mathcal{G}_k^{\text{est}} |\rho_j^{\text{est}}\rangle\rangle = \langle\langle O_i| \prod_k \mathcal{G}_k |\rho_j\rangle\rangle. \quad (\text{C7})$$

Throughout this paper, we will refer to the transformation due to SPAM errors and the  $B$  matrix as gauge and denote  $G_a$ . In the aforementioned case,  $G_a = BA^{(\text{in})-1}$ .

We remark that the choice of the gauge is crucial because it affects the set of required QEM operations; on the other hand, QEM operations are restricted to Pauli operations due to the use of the Pauli frame. Therefore, we need to carefully choose the gauge so that only Pauli operations are used for QEM. We then propose to estimate the gate set, initial states, and measurements as

$$\begin{aligned} \mathcal{G}_k^{\text{est}} &= \tilde{\mathcal{G}}g^{-1} = A^{(\text{out})}\mathcal{G}_kA^{(\text{out})-1} \\ |\rho_j^{\text{est}}\rangle\rangle &= g_{\bullet,j} = A^{(\text{out})}|\rho_j\rangle\rangle \\ \langle\langle O_i^{\text{est}}| &= \langle\langle O_i^{(0)}| = \langle\langle O_i|A^{(\text{out})-1}. \end{aligned} \quad (\text{C8})$$

We can see  $G_a = A^{(\text{out})}$ . We will later see this choice of gauge is compatible with QEM with the Pauli frame in the presence of stochastic Pauli errors.

## 2. Probabilistic error cancellation

Here we discuss how we can derive quasi-probabilities to implement probabilistic error cancellation based on

the results of gate set tomography. In addition, we also describe this method is compatible with the Pauli frame. Assume we have obtained the estimations of gate set, initial states and measurements as follows:

$$\begin{aligned} \mathcal{G}_k^{\text{est}} &= G_a\mathcal{G}_kG_a^{-1} \\ |\rho_j^{\text{est}}\rangle\rangle &= G_a|\rho_j\rangle\rangle \\ \langle\langle O_i^{\text{est}}| &= \langle\langle O_i|G_a^{-1}. \end{aligned} \quad (\text{C9})$$

We also assume that we apply gate set tomography to basis operations for QEM and obtain estimations of them as  $\mathcal{B}_l^{\text{est}} = G_a\mathcal{B}_lG_a^{-1}$ . Denote the ideal operation as  $\mathcal{U}_k$ . We attempt to invert the estimated noise process as  $\mathcal{N}_k^{\text{est-1}} = \mathcal{U}_k\mathcal{G}_k^{\text{est-1}} = \sum_l q_l\mathcal{B}_l^{\text{est}}$ . In reality, what we implement via probabilistic error cancellation corresponds to  $\mathcal{N}_k^{\text{mit-1}} = \sum_l q_l\mathcal{B}_l = G_a^{-1}\mathcal{U}_kG_a\mathcal{G}_k^{-1}$ . Therefore, the error-mitigated gate can be expressed as  $\mathcal{G}_k^{\text{mit}} = \mathcal{N}_k^{\text{mit-1}}\mathcal{G}_k = G_a^{-1}\mathcal{U}_kG_a$ . Similarly, we try to construct the ideal initial states and measurements as  $|\rho_j^{(0)}\rangle\rangle = \sum_{l'} q_{l'}\mathcal{B}_{l'}^{\text{est}}|\rho_j^{\text{est}}\rangle\rangle$  and  $\langle\langle O_i^{(0)}| = \sum_{l''} q_{l''}\langle\langle O_i^{\text{est}}|\mathcal{B}_{l''}^{\text{est}}$ , which actually correspond to  $|\rho_j^{\text{mit}}\rangle\rangle = G_a|\rho_j^{(0)}\rangle\rangle$  and  $\langle\langle O_i^{\text{mit}}| = \langle\langle O_i^{(0)}|G_a^{-1}$ , respectively. Then we obtain the error-mitigated expectation value for a sequence of quantum gates as

$$\langle\langle O_i^{\text{mit}}| \prod_k \mathcal{G}_k^{\text{mit}} |\rho_j^{\text{mit}}\rangle\rangle = \langle\langle O_i^{(0)}| \prod_k \mathcal{U}_k |\rho_j^{(0)}\rangle\rangle. \quad (\text{C10})$$

Now, we discuss compatibility of this method with the Pauli frame. We remark that when using the Pauli frame for QEM, only Pauli operations are allowed. This indicates that the solution of

$$\mathcal{N}_k^{\text{est-1}} = \sum_l q_l\mathcal{B}_l^{\text{est}} \quad (\text{C11})$$

only contains Pauli operators. Here, we choose the gauge  $G_a = A^{(\text{out})}$ . Note that in the presence of stochastic Pauli errors for measurement errors,  $A^{(\text{out})}$  can also be described by a diagonal matrix corresponding to a stochastic Pauli error. We can easily check Pauli operations are invariant under this gauge and  $\mathcal{N}_k^{\text{est-1}}$  is also described by stochastic Pauli noise when the gates suffer stochastic Pauli errors. Thus, only Pauli operators are required for QEM. Similarly, we can also show we only require Pauli operations to realize  $|\rho_j^{(0)}\rangle\rangle = \sum_{l'} q_{l'}\mathcal{B}_{l'}^{\text{est}}|\rho_j^{\text{est}}\rangle\rangle$  and  $\langle\langle O_i^{(0)}| = \sum_{l''} q_{l''}\langle\langle O_i^{\text{est}}|\mathcal{B}_{l''}^{\text{est}}$  in the presence of stochastic Pauli errors for state preparation. Therefore, this method is fully compatible with the Pauli frame.

## 3. Efficiency of gate set tomography for decoding errors

In this section, we discuss the efficiency of gate set tomography on decoding errors. Here, we assume that a target gate  $\mathcal{G}_k$  is Clifford and assume that gate and

SPAM noise are modeled as Markovian and stochastic Pauli where its error probabilities are small, i.e.,  $p_L \ll 1$ . Then, we show that we can determine each element of  $\tilde{\mathcal{G}}$  and  $g$  with a standard error  $\delta$  with  $O(\delta^{-2}p_L)$  samplings. We also show that when the estimated noise map is formed as  $\mathcal{N}_k = (1 - \varepsilon_k)\mathcal{I} + \varepsilon_k\mathcal{E}_k$  where  $\varepsilon_k = O(p_L)$ , we can estimate  $\varepsilon_k$  within the precision of  $(1 \pm r)\varepsilon_k$  with  $O(r^{-2}p_L^{-1})$  samplings.

When there was no noise, every element of  $\tilde{\mathcal{G}}$  and  $g$  is performed as a Pauli measurement for a stabilizer state. Each element is zero if a measured state is not an eigenstate of an observable, and  $\pm 1$  otherwise. Since noise is modeled as stochastic Pauli, if an element is zero without noise, then the element is also zero with noise. Thus, we do not need to perform sampling for such elements. When elements are  $\pm 1$  without noise, elements with noise become  $\pm(1 - 2\mu)$ , which is obtained as a mean value of random variable  $\hat{m}$  such that  $\hat{m} = \pm 1$  with probability  $1 - \mu$  and  $\hat{m} = \mp 1$  with probability  $\mu$  where  $\mu = O(p_L)$ . When we perform  $N_{\text{GST}}$  samplings for this distribution,  $\pm(1 - 2\mu)$  can be estimated with a standard error  $O\left(\sqrt{pN_{\text{GST}}^{-1}}\right)$ . Therefore, to estimate each element of  $\tilde{\mathcal{G}}$  and  $g$  with a standard error  $\delta$ , it enough to perform  $N_{\text{GST}} = O(\delta^{-2}p_L)$  samplings.

Suppose we obtain  $\tilde{\mathcal{G}}$  and  $g$  with small statistical fluctuation as  $\tilde{\mathcal{G}} + \Delta\tilde{\mathcal{G}}$  and  $g + \Delta g$ , respectively. Then, we show estimation of gate set tomography shown in Eq. (C8) are performed also with small standard errors.  $|\rho_j^{\text{est}}\rangle\rangle$  can be obtained directly from  $g$ , and  $\langle\langle O_i^{\text{est}}|\rangle\rangle$  can be obtained without statistical errors.  $\mathcal{G}_k^{\text{est}}$  is obtained as  $\mathcal{G}_k^{\text{est}} = (\tilde{\mathcal{G}} + \Delta\tilde{\mathcal{G}})(g + \Delta g)^{-1} \sim \tilde{\mathcal{G}}g^{-1} + \Delta\tilde{\mathcal{G}}g^{-1} - \tilde{\mathcal{G}}g^{-1}\Delta gg^{-1}$ . Thus elements of  $\mathcal{G}_k^{\text{est}}$  are also obtained with a standard error in the same order.

The noise map of  $\mathcal{G}_k^{\text{est}}$  can be obtained as  $\mathcal{N}_k = \mathcal{G}_k^{\text{est}}(\mathcal{G}_k^{(0)})^{-1}$  where  $\mathcal{G}_k^{(0)}$  is an error-free gate. Since a gauge operator is chosen so that the Pauli transfer matrix of noise map becomes diagonal,  $\mathcal{N}_k$  corresponds to a stochastic Pauli map  $\rho \mapsto \sum_{g \in \{I, X, Y, Z\}} p_g g \rho g$ . The logical error probabilities  $\{p_X, p_Y, p_Z\}$  can be obtained as a decrease of diagonal elements of  $\mathcal{N}_k$ . Let  $p_g^{\text{est}}$  for  $g \in \{X, Y, Z\}$  be an estimated logical error. Then, to achieve an estimation accuracy in the form of  $p_g^{\text{est}} = (1 + r)p_g$ , its standard error must be smaller than  $rp_g$ . Thus, the number of required samples to achieve an accuracy  $r$  in the above form is given by  $N_{\text{GST}} = O((rp_L)^{-2}p_L) = O(r^{-2}p_L^{-1})$ .

#### Appendix D: Surface code and lattice surgery

While an applicable scope of our proposal is not limited to a specific architecture of FTQC, we consider FTQC with surface codes and lattice surgery as an example. Surface code [40, 54] is considered as one of the most promising quantum error-correcting codes for integrated devices such as superconducting qubits. This is because

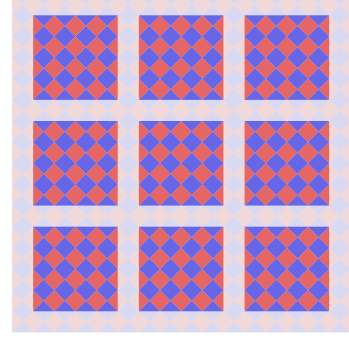


FIG. 9. The schematic of 9 logical qubits for  $d = 5$  surface code. Vertices of blue and red squares are corresponding to physical qubits. A bold patch consisting of blue and red faces represents a single logical qubit. In each logical qubit, each bold red and blue face represents Pauli-Z and Pauli-X stabilizer operators acting on its vertices, respectively.

surface code has a large threshold value, and its stabilizer measurements can be done in a short and constant depth, and it requires physical qubits that are allocated in a two-dimensional grid and interact only with the nearest neighboring ones. An array of logical qubits is shown in Fig. 9. There are 9 deeply colored patches in the figure, each of which corresponds to a logical qubit. Data qubits are allocated on vertices of deep red and blue faces. Red and blue faces in each patch correspond to stabilizer operators which act on its vertices as Pauli-Z and Pauli-X operators, respectively. The width of a deeply colored patch  $d$  is equivalent to a code distance. Thus, we use  $O(d^2)$  physical qubits per logical qubit for surface codes with code distance  $d$ . Note that while we can reduce the number of physical qubits by using rotated surface codes [6], we use surface codes shown in Fig. 9 for a simple numerical simulation.

Meanwhile, lattice surgery [6, 7] is a method to increase the number of logical qubits and perform logical two-qubit gates with physical qubits on planer topology. When we prepare logical qubits as patches, we can perform Hadamard gate transversally. Although a logical CNOT-gate is also transversal in surface codes, we cannot perform it fault-tolerantly in planer topology. Instead, we implement multi-qubit Pauli measurements by merging and splitting patches corresponding to logical qubits. By using multi-qubit Pauli measurements and feed-forward operations, we can indirectly perform logical two-qubit Clifford gates fault-tolerantly. For non-transversal operations, we can perform them by inject, distill, and consume two types of magic states  $|A\rangle$  and  $|Y\rangle = SH|0\rangle$  where  $S = \exp(i\frac{\pi}{4}Z)$ . Using these magic states and a technique of gate teleportation, we can indirectly apply non-transversal operations such as  $S$ -gate and  $T$ -gate. While we can perform  $S$ -gate using  $|Y\rangle$  without consuming it, a magic state  $|A\rangle$  for  $T$ -gate is consumed in each application. Therefore, the number of

required  $|A\rangle$  is a dominant factor in the execution time.

Although we choose a strategy of FTQC mentioned above in the main text, there are several other possible strategies for the choice of codes and logical operations to improve efficiency and feasibility. We can also construct logical qubits as defect-pairs in a single large patch and perform two-qubit Clifford gates with braiding [5]. We can also use concatenated Steane codes or color codes if we can perform CNOT operations more flexibly.  $S$ -gate can be achieved with code deformation [55] instead of magic state injection and distillation. We can choose  $CCZ$ -gate as a magic state instead of  $T$ -gate [56]. We can estimate recovery operations with algorithms that achieve small latency with threshold degradation [39, 57]. In any case, our method is general; therefore we expect our proposal can be applied naturally.

### Appendix E: Concrete process for logical operations

In this section, we explicitly explain how our framework works by updating the quantum state of experimental devices and the Pauli frame, i.e., a classical memory for storing and updating Pauli operators for obtaining error-corrected results via post-processing of measurement outcomes. Note that we have a latency to collect sufficient information to correct quantum states since there are errors in syndrome measurements and we cannot instantaneously perform feedback operations for error correction; the required recovery Pauli operations need to be ceaselessly updated in the Pauli frame classically because unitary Clifford operators for computation are performed while storing outcomes of syndrome measurements. Finally, we can obtain the error-corrected results by post-processing measurement outcomes based on the state of the Pauli frame.

First, we describe a typical construction of FTQC without QEM studied in Refs. [7, 34]. We reformulate them with the superoperator representation for introducing notations that simplifies the description of our framework. Then, we explain our FTQC framework incorporating both QEC and QEM. More specifically, decoding errors are assumed to be not negligible and are mitigated by probabilistic error cancellation on the logical space.

In FTQC, a process of syndrome measurements on the whole logical qubits is called *code cycle*. For reliable decoding, we need to wait for several cycles according to the code distance before processing the next logical operation. For a plain notation, we call a unit of the latency for the slowest logical operation (i.e. the maximum number of cycles that required for being ready for the next logical operation) as *step*, and assume that in each logical operation, every logical qubit waits until all the logical qubits become ready for the next logical operations. This enables a simple definition of the states of quantum devices and classical memory at a certain step. We emphasize that this unit is introduced only for the readability of our manuscript and our scheme can be applied

to asynchronous processing of logical operations.

### 1. FTQC architecture without QEM

At the  $t$ -th step of FTQC without QEM, we have two components to be updated: a quantum device of which the state is  $|\rho_{\text{dev}}^{(t)}\rangle$  and the Pauli frame  $\mathcal{P}_{\text{PF}}^{(t)}$ . Suppose that the Pauli transfer matrix of an actual quantum process that suffers noise until the  $t$ -th step is  $\mathcal{U}_{\text{dev}}^{(t)}$  and an ideal initial state as  $|\rho_0\rangle$ . Then, the state at the  $t$ -th step can be represented as  $|\rho_{\text{dev}}^{(t)}\rangle = \mathcal{U}_{\text{dev}}^{(t)}|\rho_0\rangle$ . Note that  $\mathcal{U}_{\text{dev}}^{(t)}$  is the superoperator of a trace-preserving and completely positive map but is not a unitary process since the actual process require several intermediate measurements. Denote the ideal operations until the  $t$ -step as  $\tilde{\mathcal{U}}^{(t)}$ . Here, we aim to have

$$\mathcal{P}_{\text{PF}}^{(t)}\mathcal{U}_{\text{dev}}^{(t)} = \tilde{\mathcal{U}}^{(t)} \quad (\text{E1})$$

for an arbitrary step  $t$ . Note that since several successive syndrome values are required to calculate  $\mathcal{P}_{\text{PF}}^{(t)}$ , the Pauli frame at the  $t$ -th step turns out at least with a latency of cycles proportional to the code distance [34].

In this manuscript, we focus on a simplified universal set of logical operations: preparation of logical  $|0_L\rangle$  and  $|A_L\rangle$ , logical Clifford operations including logical Pauli operations, logical single-qubit Pauli- $Z$  measurements, and logical gate teleportation for performing a logical  $T$ -gate. While these logical operations can be divided into more basic logical operations such as merge-and-split operations in a lattice surgery [6], we use the above set for simplicity. In the following, we illustrate how the physical states and the Pauli frame are updated in each case.

#### a. Preparation of logical states

There are two types of initialization in FTQC: preparation of a logical  $|0_L\rangle$  state and a logical magic state  $|A_L\rangle$  implemented in the surface code. Here, we describe an operation to add a clean logical qubit as

$$\begin{aligned} \mathcal{Q}_0|\rho\rangle &:= |\rho\rangle \otimes |0_L\rangle \\ \mathcal{Q}_A|\rho\rangle &:= |\rho\rangle \otimes |A_L\rangle \end{aligned} \quad (\text{E2})$$

Let us first explain the procedure of preparation of  $|0_L\rangle$ . We join  $n$  physical qubits to a system, where  $n$  is a number of qubits to construct a logical qubit. The initial state of joined data qubits can be any random state. We measure all the joined data qubits with Pauli- $Z$  basis. If there is no error in this measurement, we obtain a computational basis  $|\mathbf{x}\rangle$  where  $\mathbf{x} \in \{0, 1\}^n$  is  $n$ -bit outcomes. We suppose a Pauli operator  $P_{\mathbf{x}} = \bigotimes_i X^{x_i}$ , then we find  $P_{\mathbf{x}}|\mathbf{x}\rangle = |0\rangle^{\otimes n}$ . The state  $|0\rangle^{\otimes n}$  is a +1 eigenstate of all the  $Z$ -stabilizer operators and logical Pauli- $Z$

operator, but not an eigenstate of any  $X$ -stabilizer operators. We perform  $X$ -stabilizer measurements to project  $|0\rangle^{\otimes n}$  to the code space. If the state is projected to  $+1$  eigenspace for all the  $X$ -stabilizer operators, the state becomes  $+1$  eigenstate of all the stabilizer operators and logical Pauli- $Z$  operator, which is the definition of  $|0_L\rangle$ . If any of them are  $-1$ , we can find a Pauli- $Z$  operator  $P_z$  which anti-commutes with all the  $X$ -stabilizer operators with  $-1$  outcome and commutes with the other stabilizer operators. Then, we see  $P_z P_x |\psi\rangle$ , where  $|\psi\rangle$  is a state after  $X$ -stabilizer measurements on  $|\mathbf{x}\rangle$ , is equal to  $|0\rangle_L$ . As a result, a procedure to add  $|0_L\rangle$  is described as follows:  $\mathcal{U}_{\text{dev}}^{(t+1)}$  is a sequence to join  $n$ -qubits, measure all of them in Pauli- $Z$  basis, and perform  $X$ -stabilizer measurements. The Pauli frame  $\mathcal{P}_{\text{PF}}^{(t+1)}$  is a tensor product of  $\mathcal{P}_{\text{PF}}^{(t)}$  and the superoperator of  $P_z P_x$ . In practice, there may be Pauli errors during the above measurements. Since these error rates are expected to be below the threshold value, they can be reliably detected in the successive stabilizer measurements and corrected by updating  $P_z P_x$ . See Sec. E 1 c for an update of the Pauli frame with a latency.

The other initialization is a logical magic state  $|A_L\rangle$ , which is, as detailed later, used for performing non-Clifford gates fault-tolerantly via gate teleportation. For the use of gate teleportation, the infidelity of a logical magic state must be comparable to or smaller than the required logical error rate. On the other hand, since  $|A_L\rangle$  is not an eigenstate of logical Pauli- $Z$  operator nor logical Pauli- $X$  operator, we cannot use the same preparation method for  $|0_L\rangle$ . Instead, a logical magic state  $|A_L\rangle$  with a fidelity enough for gate teleportation is constructed by the following three steps: I) Create a noisy magic state  $|A_L\rangle$  whose code distance is a small constant  $d_s$ , II) Expand a code distance from  $d_s$  to  $d$  fault-tolerantly, and III) Create a clean magic state from several noisy magic states with magic state distillation. If the fidelity of noisy magic states is sufficiently large and a magic state is sufficiently distilled, we can obtain a clean magic state together with its Pauli frame. For a detail of these procedure, see Refs. [7, 34, 58].

Then, we can perform an update  $\tilde{\mathcal{U}}^{(t+1)} = \mathcal{Q}\tilde{\mathcal{U}}^{(t)}$  where  $\mathcal{Q} \in \{\mathcal{Q}_0, \mathcal{Q}_A\}$  by updating  $\mathcal{U}_{\text{dev}}^{(t)}$  and  $\mathcal{P}_{\text{PF}}^{(t)}$  as

$$\begin{aligned}\mathcal{U}_{\text{dev}}^{(t+1)} &= (\mathcal{I} \otimes \mathcal{P}_{\text{PF}}^{(Q)}) \mathcal{Q} \mathcal{U}_{\text{dev}}^{(t)} \\ \mathcal{P}_{\text{PF}}^{(t+1)} &= \mathcal{P}_{\text{PF}}^{(t)} \otimes \mathcal{P}_{\text{PF}}^{(Q)}\end{aligned}\quad (\text{E3})$$

where  $\mathcal{P}_{\text{PF}}^{(Q)}$  turns out with a latency because of noisy syndrome measurements.

### b. Logical Pauli Operation

Logical Pauli operations are special cases of logical Clifford operations and can be performed much more easily than general Clifford operations due to the Pauli frame. When we perform a logical Pauli operation  $\mathcal{P}^{(t)}$

at the  $t$ -th step, we need to construct  $\mathcal{P}_{\text{PF}}^{(t+1)}$  and  $\mathcal{U}_{\text{dev}}^{(t+1)}$  such that  $\mathcal{P}_{\text{PF}}^{(t+1)} \mathcal{U}_{\text{dev}}^{(t+1)} = \tilde{\mathcal{U}}^{(t+1)} = \mathcal{P}^{(t)} \tilde{\mathcal{U}}^{(t)}$ . Since a logical Pauli operation is a product of physical Pauli operations, there are two ways to achieve this. One is to update only the Pauli frame as follows:

$$\begin{aligned}\mathcal{P}_{\text{PF}}^{(t+1)} &= \mathcal{P}^{(t)} \mathcal{P}_{\text{PF}}^{(t)} \\ \mathcal{U}_{\text{dev}}^{(t+1)} &= \mathcal{U}_{\text{dev}}^{(t)}\end{aligned}\quad (\text{E4})$$

Note that this is an instant and noiseless operation because it is processed only on the classical computer. We refer to this scheme as a Pauli operation by *software update*.

The other is to update the physical device instead of the Pauli frame.

$$\mathcal{P}_{\text{PF}}^{(t+1)} = \mathcal{P}_{\text{PF}}^{(t)} \quad (\text{E5})$$

$$\mathcal{U}_{\text{dev}}^{(t+1)} = \mathcal{P}^{(t)} \mathcal{U}_{\text{dev}}^{(t)} \quad (\text{E6})$$

Compared to the software update, this operation requires an operation on the physical quantum devices, and hence this operation may involve an error. We call this scheme a *hardware update*. Note that this procedure is a transversal single-qubit Pauli operation, we expect this operation increases negligibly a physical error rate per code cycle. Although there seems no advantage in the hardware update in a typical architecture of FTQC, logical Pauli operations by hardware update is required in the Pauli twirling of logical errors on FTQC as described in Appendix. F.

### c. Logical Clifford Operation

Unlike logical Pauli operations, we need a physical operation to quantum devices to perform logical Clifford operations. We denote the Pauli transfer matrix of physical errors at the  $t$ -th step as  $\mathcal{P}_{\text{rec}}^{(t)}$ . Note that since quantum states are projected to the code space with syndrome measurements, we expect  $\mathcal{P}_{\text{rec}}^{(t)}$  is approximated as a Pauli error. For the case where we cannot assume  $\mathcal{P}_{\text{rec}}^{(t)}$  as a Pauli error, we can twirl it with stochastic Pauli operations with hardware update and project it to stochastic Pauli errors. See Appendix. F for details.

Pauli errors are detected via syndrome measurements, and a recovery Pauli operation  $\mathcal{P}_{\text{rec}}^{(t)}$  is estimated with a high success probability and the Pauli frame is updated in the same way as Eq. (E4). If there are no measurement errors, the recovery operation for a certain cycle is estimated only from syndrome values at the same cycle. However, when syndrome measurements suffer physical errors, we need to idle logical qubits for  $d$  cycles to collect sufficient syndrome measurement outcomes before starting the next Clifford operation to guarantee the exponential decay of logical error rates [34]. Therefore, the recovery operations turn out with a latency of at least  $d$  cycles. In practice, the latency is larger than  $d$  cycles

since we further need post-processing for signal discrimination and decoding algorithms on classical peripherals.

Suppose we perform logical Clifford operation  $\mathcal{C}^{(t)}$ . Physical Pauli errors  $\mathcal{P}_{\text{rec}}^{(t)}$  happens during the Clifford operation, which turns out later by decoding. Here, we ignore a failure of recovery, assuming the code distance is sufficiently large. We aim to obtain  $\mathcal{P}_{\text{PF}}^{(t+1)}$  and  $\mathcal{U}_{\text{dev}}^{(t+1)}$  that satisfy  $\mathcal{P}_{\text{PF}}^{(t+1)}\mathcal{U}_{\text{dev}}^{(t+1)} = \tilde{\mathcal{U}}^{(t+1)} = \mathcal{C}^{(t)}\tilde{\mathcal{U}}^{(t)}$ . An action of logical Clifford operation updates the state of quantum devices as follows:

$$\mathcal{U}_{\text{dev}}^{(t+1)} = \mathcal{P}_{\text{rec}}^{(t)}\mathcal{C}^{(t)}\mathcal{U}_{\text{dev}}^{(t)}. \quad (\text{E7})$$

$$\begin{aligned} \mathcal{P}_{\text{PF}}^{(t+2)} &= \mathcal{P}_{\text{rec}}^{(t+1)}\mathcal{C}^{(t+1)}\mathcal{P}_{\text{PF}}^{(t+1)}(\mathcal{C}^{(t+1)})^{-1} \\ &= (\mathcal{C}^{(t+1)}\mathcal{C}^{(t)}\mathcal{P}_{\text{PF}}^{(t)}(\mathcal{C}^{(t)})^{-1}(\mathcal{C}^{(t+1)})^{-1})(\mathcal{C}^{(t+1)}\mathcal{P}_{\text{rec}}^{(t)}(\mathcal{C}^{(t+1)})^{-1})\mathcal{P}_{\text{rec}}^{(t+1)}. \end{aligned} \quad (\text{E9})$$

Since Pauli actions commute, we can update a part  $\mathcal{C}^{(t+1)}\mathcal{P}_{\text{rec}}^{(t)}(\mathcal{C}^{(t+1)})^{-1}$  even at the next step. We can use the similar technique when the next operation is a logical Pauli measurement, which is explained in the next section. Therefore, as far as all the successive operations are Clifford operations or Pauli measurements, we can postpone an application of recovery operators and updates of the Pauli frame. This technique is essential not only for improving the throughput of logical operations in FTQC but also for avoiding an exponential growth of latency [57].

Note that in the scheme of lattice surgery, logical CNOTs are achieved with the preparation of logical  $|0_L\rangle$  state, three two-qubit logical Pauli measurements, and three adaptive Pauli operations [7]. While each of them is not a Clifford operation, we can consider the whole of them as a unitary process. An application of adaptive Pauli operations can be postponed for the same reason as the updates of the Pauli frame.

#### d. Single-qubit logical Pauli measurement

We can perform a destructive single-qubit logical Pauli- $Z$  measurement by physical Pauli- $Z$  measurements on all the data qubits of a target logical qubit. Note that logical Pauli measurements with the other Pauli basis can be achieved by swapping  $Z$  and  $X$  or combining with single-qubit Logical Clifford operations. The outcome of a logical measurement is calculated as the parity of measurement outcomes of the data qubits. In other words, let  $n$  be the number of data qubits of the target logical

Besides that, we update a Pauli frame as follows:

$$\mathcal{P}_{\text{PF}}^{(t+1)} = \mathcal{C}^{(t)}\mathcal{P}_{\text{PF}}^{(t)}(\mathcal{C}^{(t)})^{-1}\mathcal{P}_{\text{rec}}^{(t)}. \quad (\text{E8})$$

Since logical Clifford operation is also a Clifford operation for physical qubits in the cases of stabilizer codes,  $\mathcal{P}_{\text{PF}}^{(t+1)}$  is a Pauli operator.

In practice,  $\mathcal{P}_{\text{rec}}^{(t)}$  is expected to turn out with a large latency since it requires post-processing to estimate a recovery operation. Thus, another Pauli error would happen during idling operations to wait for estimation of  $\mathcal{P}_{\text{rec}}^{(t)}$ . Nevertheless, the next logical Clifford operation or logical Pauli measurements can be performed before  $\mathcal{P}_{\text{rec}}^{(t)}$  turns out. As an example, we show a case when  $\mathcal{C}^{(t+1)}$  is processed before the last Pauli frame is updated. Then, the Pauli frame of the next step is represented as

qubit, and  $\Pi_{\mathbf{x}} = \prod_i (I + (-1)^{x_i} Z_i)/2$  for  $\mathbf{x} \in \{0, 1\}^n$  be an operator that projects all the data qubits in a physical computational basis  $|\mathbf{x}\rangle$ . A single-bit outcome of a single-qubit logical measurement is calculated as a parity of the outcomes of physical measurements  $\mathbf{x}$ . We denote this function as  $f : \{0, 1\}^n \rightarrow \{0, 1\}$ . Therefore, we aim to estimate  $\mathbf{x}$  and obtain  $f(\mathbf{x})$  fault tolerantly.

When we perform physical Pauli- $Z$  measurements, physical Pauli errors  $\mathcal{P}_{\text{rec}}^{(t)}$  occur on the data qubits. Also, as explained in the section of logical Clifford operations, the Pauli frame  $\mathcal{P}_{\text{PF}}^{(t)}$  does not turn out at the timing of the logical measurement. Even in this case, the recovery operation can be applied even after physical Pauli- $Z$  measurements are performed on the data qubits since

$$\begin{aligned} \langle \langle \Pi_{\mathbf{x}} | \mathcal{P}_{\text{rec}}^{(t)} \mathcal{U}_{\text{dev}}^{(t)} = \langle \langle \Pi_{\mathbf{x} \oplus \mathbf{y}} | \mathcal{P}_{\text{PF}}^{(t)} \mathcal{U}_{\text{dev}}^{(t)} \\ = \langle \langle \Pi_{\mathbf{x} \oplus \mathbf{y}} | \tilde{\mathcal{U}}^{(t)} \end{aligned} \quad (\text{E10})$$

where  $\oplus$  represents an element-wise XOR, and  $\mathbf{y} \in \{0, 1\}^n$  is a binary vector such that  $y_i = 1$  if  $\mathcal{P}_{\text{PF}}^{(t)}\mathcal{P}_{\text{rec}}^{(t)}$  acts on the  $i$ -th data qubits as Pauli- $X$  or  $Y$  and  $y_i = 0$  otherwise. We denote this function as  $\mathbf{y} = \text{mask}(\mathcal{P}_{\text{PF}}^{(t)}\mathcal{P}_{\text{rec}}^{(t)})$ .

Therefore, we obtain  $\mathbf{x}$  as an outcome of the measurement on the uncorrected state  $|\rho_{\text{dev}}^{(t)}\rangle$ . Notice that  $\mathbf{y}$  turns out when the decoding process catches up with the code cycle of logical measurements, and we can retrieve the error-corrected logical outcome as  $f(\mathbf{x} \oplus \text{mask}(\mathcal{P}_{\text{PF}}^{(t)}\mathcal{P}_{\text{rec}}^{(t)}))$ . The update rules can be written as

$$\mathcal{U}_{\text{dev}}^{(t+1)} = \frac{1}{p_{\mathbf{x}}} \langle \langle \Pi_{\mathbf{x}} | \mathcal{P}_{\text{rec}}^{(t)} \mathcal{U}_{\text{dev}}^{(t)} \quad (\text{E11})$$

$$\mathcal{P}_{\text{PF}}^{(t+1)} = \text{Dis}_M[\mathcal{P}_{\text{PF}}^{(t)}], \quad (\text{E12})$$

where  $p_{\mathbf{x}}$  is the probability with which we obtain  $\mathbf{x}$ ,  $\text{Dis}_M[\cdot]$  is an operation to discard the Pauli frame corresponding to the measured logical qubits. In contrast to the logical initialization, this update will remove the logical space by destructive measurements.

Several things should be noted on the decoding algorithm at the measurement timing. A Pauli frame can be represented as the form of  $(\bigotimes_i X^{x_i} Z^{z_i})$  for  $x_i, z_i \in \{0, 1\}$ . We call  $\{x_i\}$  and  $\{z_i\}$  as a  $X$ -part and  $Z$ -part of the Pauli frame, respectively. Since all the data qubits are directly measured in this logical operation, syndrome measurements are not performed in this code cycle. Instead, we can calculate the values of  $Z$ -stabilizer syndrome measurements without measurement errors as parities of  $\mathbf{x}$  because we directly measure data qubits without resorting to ancilla qubits. Since there is no effective measurement error in  $Z$ -stabilizer syndrome measurements at the cycle of the logical measurement, an estimation of the  $X$ -part of  $\mathcal{P}_{\text{PF}}^{(t)}\mathcal{P}_{\text{rec}}^{(t)}$  can be converted to an instance of a graph problem called minimum-weight perfect matching [34]. On the other hand, the information required to construct a perfect matching problem for estimating the  $Z$ -part of the Pauli frame is lost by the direct  $Z$ -basis measurements. Nevertheless, this does not affect the computation since only the  $X$ -part of the Pauli frame

is relevant to know  $\mathbf{y} = \text{mask}(\mathcal{P}_{\text{PF}}^{(t)}\mathcal{P}_{\text{rec}}^{(t)})$ .

e. *Gate teleportation with magic state*

For a universal FTQC, we need to perform non-Clifford operations to logical qubits encoded in the surface code. To this end, in a typical scenario, we create a logical qubit prepared in  $|A_L\rangle\rangle$ , and perform  $T$ -gate on the target system by consuming a magic state  $|A_L\rangle\rangle$ .

First, we describe a gate teleportation without noise. Let  $|\rho\rangle\rangle \otimes |A\rangle\rangle$  be a tensor product of a target system and a magic state. It is known that the following equation holds for an arbitrary  $\rho$  [34, 59]:

$$(\mathcal{S}^{f(\mathbf{x})} \otimes \langle\langle \Pi_{\mathbf{x}} | \Lambda \mathcal{Q}_A | \rho \rangle\rangle) = (\mathcal{S}^{f(\mathbf{x})} \otimes \langle\langle \Pi_{\mathbf{x}} | \Lambda (|\rho\rangle\rangle \otimes |A_L\rangle\rangle) = \mathcal{T} |\rho\rangle\rangle \langle\langle \Pi_{\mathbf{x}} | +_L \rangle\rangle, \quad (\text{E13})$$

where  $\Lambda$  is the Pauli transfer matrix of a logical CNOT-gate which acts on  $|\rho\rangle\rangle$  as a control and  $|A_L\rangle\rangle$  as a target,  $\mathcal{T}$  is the Pauli transfer matrix of  $T$ -gate, and  $\mathcal{S}^{f(\mathbf{x})}$  is the Pauli transfer matrix of an adaptive  $S$ -gate that is applied on the state if  $f(\mathbf{x}) = 1$  (for the definition of function  $f$ , see the last section).

Using the above fact, we can construct the following update rules for the target system as

$$\mathcal{U}_{\text{dev}}^{(t+1)} = \frac{1}{p_{\mathbf{x}}} (\mathcal{S}^{f(\mathbf{x} \oplus \mathbf{y})} \otimes \langle\langle \Pi_{\mathbf{x}} | \mathcal{P}_{\text{rec}}^{(t)} \Lambda (\mathcal{I} \otimes \mathcal{P}_{\text{PF}}^{(Q)}) \mathcal{Q}_A \mathcal{U}_{\text{dev}}^{(t)} \rangle\rangle) \quad (\text{E14})$$

$$\mathcal{P}_{\text{PF}}^{(t+1)} = \mathcal{S}^{f(\mathbf{x} \oplus \mathbf{y})} \text{Dis}_Q [\Lambda (\mathcal{P}_{\text{PF}}^{(t)} \otimes \mathcal{P}_{\text{PF}}^{(Q)}) \Lambda^{-1} \mathcal{P}_{\text{rec}}^{(t)}] \mathcal{S}^{-f(\mathbf{x} \oplus \mathbf{y})}, \quad (\text{E15})$$

where  $\mathcal{P}_{\text{rec}}^{(t)}$  is a detectable physical errors,

$$p_{\mathbf{x}} = \langle\langle \Pi_{\mathbf{x} \oplus \mathbf{y}} | +_L \rangle\rangle, \quad (\text{E16})$$

$$\mathbf{y} = \text{mask}(\text{Dis}_\rho [\Lambda (\mathcal{P}_{\text{PF}}^{(t)} \otimes \mathcal{P}_{\text{PF}}^{(Q)}) \Lambda^{-1} \mathcal{P}_{\text{PF}}^{(t)}]), \quad (\text{E17})$$

and  $\text{Dis}_Q[\cdot]$  ( $\text{Dis}_\rho[\cdot]$ ) is an operation to discard the Pauli frame of the magic state (target state). Then, we can verify the above update rule keeps Eq. (E4) as follows.

$$\begin{aligned} \mathcal{P}_{\text{PF}}^{(t+1)} \mathcal{U}_{\text{dev}}^{(t+1)} &= \frac{1}{p_{\mathbf{x}}} \mathcal{S}^{f(\mathbf{x} \oplus \mathbf{y})} \text{Dis}_Q [\Lambda (\mathcal{P}_{\text{PF}}^{(t)} \otimes \mathcal{P}_{\text{PF}}^{(Q)}) \Lambda^{-1} \mathcal{P}_{\text{rec}}^{(t)}] \mathcal{S}^{-f(\mathbf{x} \oplus \mathbf{y})} (\mathcal{S}^{f(\mathbf{x} \oplus \mathbf{y})} \otimes \langle\langle \Pi_{\mathbf{x}} | \mathcal{P}_{\text{rec}}^{(t)} \Lambda (\mathcal{I} \otimes \mathcal{P}_{\text{PF}}^{(Q)}) \mathcal{Q}_A \mathcal{U}_{\text{dev}}^{(t)} \rangle\rangle) \\ &= \frac{1}{p_{\mathbf{x}}} (\mathcal{S}^{f(\mathbf{x} \oplus \mathbf{y})} \otimes \langle\langle \Pi_{\mathbf{x}} | \text{Dis}_Q [\Lambda (\mathcal{P}_{\text{PF}}^{(t)} \otimes \mathcal{P}_{\text{PF}}^{(Q)}) \Lambda^{-1} \mathcal{P}_{\text{rec}}^{(t)}] \mathcal{P}_{\text{rec}}^{(t)} \Lambda (\mathcal{I} \otimes \mathcal{P}_{\text{PF}}^{(Q)}) \mathcal{Q}_A \mathcal{U}_{\text{dev}}^{(t)} \rangle\rangle) \\ &= \frac{1}{p_{\mathbf{x}}} (\mathcal{S}^{f(\mathbf{x} \oplus \mathbf{y})} \otimes \langle\langle \Pi_{\mathbf{x} \oplus \mathbf{y}} | \rangle\rangle) (\Lambda (\mathcal{P}_{\text{PF}}^{(t)} \otimes \mathcal{P}_{\text{PF}}^{(Q)}) \Lambda^{-1} \mathcal{P}_{\text{rec}}^{(t)} \mathcal{P}_{\text{rec}}^{(t)} \Lambda (\mathcal{I} \otimes \mathcal{P}_{\text{PF}}^{(Q)}) \mathcal{Q}_A \mathcal{U}_{\text{dev}}^{(t)}) \\ &= \frac{1}{p_{\mathbf{x}}} (\mathcal{S}^{f(\mathbf{x} \oplus \mathbf{y})} \otimes \langle\langle \Pi_{\mathbf{x} \oplus \mathbf{y}} | \rangle\rangle) \Lambda \mathcal{Q}_A \mathcal{P}_{\text{PF}}^{(t)} \mathcal{U}_{\text{dev}}^{(t)} \\ &= \mathcal{T} \tilde{\mathcal{U}}^{(t)} = \tilde{\mathcal{U}}^{(t+1)}. \end{aligned} \quad (\text{E18})$$

Note that we used the following property of the discard operation for an arbitrary Pauli operation  $\mathcal{P}$ :

$$\langle\langle \Pi_{\mathbf{x}} | = \langle\langle \Pi_{\mathbf{x} \oplus \text{mask}(\mathcal{P})} | \mathcal{P} \quad (\text{E19})$$

$$\mathcal{P} = \text{Dis}_Q[\mathcal{P}] \text{Dis}_\rho[\mathcal{P}] \quad (\text{E20})$$

Note that  $\mathbf{y}$  turns out with a latency due to the decoding process, two operations ( $\mathcal{S}^{f(\mathbf{x})}$  and  $\langle\langle \Pi_{\mathbf{x}} |$ ) cannot be performed simultaneously. Thus, there is an additional delay to determine  $f(\mathbf{x} \oplus \mathbf{y})$ , i.e., whether we perform  $\mathcal{S}$  or not.

## 2. FTQC architecture with QEM

When a code distance of quantum error correction is not sufficient, a failure probability of decoding is not negligible. Here, we consider the case that a decoding error  $\mathcal{N}$  follows the operation. We assume that  $\mathcal{N}$  is a stochastic logical Pauli channel that depends only on the next and previous  $d$  cycles and is efficiently characterized in advance. While these assumptions do not hold rigorously in practice, we expect this approximately holds with negligible errors in typical computing hardware. For the justification of this assumption, see Appendix F. Note that even if there is a finite discrepancy in this approximation, our scheme can decrease bias in the expectation values as far as the discrepancy is small. In this section, we show probabilistic error cancellation can be integrated into the architecture of FTQC. More concretely, we show each logical operation shown in the previous section can be modified so that probabilistic error cancellation can remove the residual noise of QEC only with additional logical Pauli operations by a software update.

Unlike the scenario of NISQ computing, operations of FTQC are probabilistic since intermediate measurements are involved for the gate teleportation of magic states,

and subsequent operations are adaptatively chosen corresponding to the measurement outcomes. We need to determine QEM operations accordingly because decoding noise processes may change depending on the measurement outcomes. Here, we denote the set of outcomes of intermediate measurements and QEM operations up to the  $t$ -th step as  $\mathbf{h}(t)$ , with the corresponding Pauli frame and the state of the hardware denoted as  $\mathcal{P}_{\text{PF}}^{(\mathbf{h}(t))}$  and  $\mathcal{U}_{\text{dev}}^{(\mathbf{h}(t))}$ . We remark that we do not independently define the set of measurement outcomes and QEM operations since they affect each other. The probability that  $\mathbf{h}(t)$  can be expressed as  $p_{\mathbf{h}(t)} q_{\mathbf{h}(t)}$ , where  $p_{\mathbf{h}(t)}$  is a probability with which a certain measurement outcomes of intermediate measurements is observed and  $q_{\mathbf{h}(t)}$  is a probability with which a certain QEM operation is performed. Note that, they are functions of  $\mathbf{h}(t)$ . Furthermore, we denote the parity of QEM operation (a product of parities of generated QEM operations) and the QEM cost at the  $t$ -th step as  $s^{(\mathbf{h}(t))}$  and  $\gamma_Q^{(\mathbf{h}(t))}$ .

In our framework, we can construct a consistent FTQC architecture incorporating QEM by satisfying the following equation:

$$\sum_{\mathbf{h}(t)} q_{\mathbf{h}(t)} p_{\mathbf{h}(t)} \gamma_Q^{(\mathbf{h}(t))} s^{(\mathbf{h}(t))} \mathcal{P}_{\text{PF}}^{(\mathbf{h}(t))} \mathcal{U}_{\text{dev}}^{(\mathbf{h}(t))} = \tilde{\mathcal{U}}^{(t)}. \quad (\text{E21})$$

Here, we explain why satisfying the above equation is sufficient. If we can construct  $\mathcal{U}_{\text{dev}}^{(\mathbf{h}(t))}$  as a product of physical processes, we can sample a density matrix  $|\rho^{(\mathbf{h}(t))}\rangle\rangle = \mathcal{P}_{\text{PF}}^{(\mathbf{h}(t))} \mathcal{U}_{\text{dev}}^{(\mathbf{h}(t))} |\rho_0\rangle\rangle$  with probability  $q_{\mathbf{h}(t)} p_{\mathbf{h}(t)}$ . Suppose the spectral decomposition of a given observable  $O$  as  $O = \sum_i O_i \Pi_i$  ( $O_i \in \mathbb{R}$ ). The sampling from the final state with POVM elements  $\{\Pi_i\}$  with weight  $\gamma_Q^{(\mathbf{h}(t))} s^{(\mathbf{h}(t))} O_i$  gives

$$\begin{aligned} \sum_{\mathbf{h}(t), i} q_{\mathbf{h}(t)} p_{\mathbf{h}(t)} \gamma_Q^{(\mathbf{h}(t))} s^{(\mathbf{h}(t))} O_i \langle\langle \Pi_i | \rho^{(\mathbf{h}(t))} \rangle\rangle &= \langle\langle O | \sum_{\mathbf{h}(t)} q_{\mathbf{h}(t)} p_{\mathbf{h}(t)} \gamma_Q^{(\mathbf{h}(t))} s^{(\mathbf{h}(t))} \mathcal{P}_{\text{PF}}^{(\mathbf{h}(t))} \mathcal{U}_{\text{dev}}^{(\mathbf{h}(t))} |\rho_0\rangle\rangle \\ &= \langle\langle O | \tilde{\mathcal{U}}^{(t)} | \rho_0 \rangle\rangle, \end{aligned} \quad (\text{E22})$$

which shows that QEM can recover a unbiased expectation value of observables when Eq. (E21) holds.

### a. Logical Pauli operation

Since logical Pauli operation by software update is an instant and noiseless operation, we do not need to consider error mitigation for them.

### b. Logical Clifford operation

We assume that we want to apply a Clifford operation  $\mathcal{C}$  at the  $(t+1)$ -th step; however, it is followed not only by detected physical Pauli errors  $\mathcal{P}_{\text{rec}}^{(t+1)}$  but also by a logical Pauli noise  $\mathcal{N}$  reflecting decoding failure with a non-negligible probability, i.e., a quantum device is updated as

$$\mathcal{U}_{\text{dev}}^{(\mathbf{h}(t+1))} = \mathcal{P}_{\text{rec}}^{(t)} \mathcal{N} \mathcal{C} \mathcal{U}_{\text{dev}}^{(\mathbf{h}(t))}. \quad (\text{E23})$$

While  $\mathcal{P}_{\text{rec}}^{(t)}$  is revealed with a latency and canceled by updating the Pauli frame,  $\mathcal{N}$  is not canceled and affects the expectation values without QEM. Here, We show that we can cancel  $\mathcal{N}$  by applying QEM with a probabilistic update of the Pauli frame. Our goal is to find a set of update rules  $(\gamma_Q^{(\mathbf{h}(t))}, s^{(\mathbf{h}(t))}, \mathcal{P}_{\text{PF}}^{(\mathbf{h}(t))}, \mathcal{U}_{\text{dev}}^{(\mathbf{h}(t))}) \mapsto (\gamma_Q^{(\mathbf{h}(t+1))}, s^{(\mathbf{h}(t+1))}, \mathcal{P}_{\text{PF}}^{(\mathbf{h}(t+1))}, \mathcal{U}_{\text{dev}}^{(\mathbf{h}(t+1))})$  which satisfies Eq. (E21) for

$$\tilde{\mathcal{U}}^{(t+1)} = \mathcal{C}\tilde{\mathcal{U}}^{(t)}. \quad (\text{E24})$$

Since we know a stochastic logical Pauli noise  $\mathcal{N}$  in advance, we can calculate the inverse of the noise map  $\mathcal{N}^{-1} = \sum_i \eta_i \mathcal{P}_i$ . We decompose a non-zero coefficient

$\eta_i$  as  $\eta_i = \gamma_Q \text{sgn}(\eta_i) q_i$  where  $\gamma_Q = \sum_i |\eta_i|$  and  $q_i = |\eta_i|/\gamma_Q$ . We randomly choose  $i$  with the probability  $q_i$ , and the index  $i$  is appended to give  $\mathbf{h}(t+1)$ . We find  $q_{\mathbf{h}(t+1)} = q_i q_{\mathbf{h}(t)}$  and  $p_{\mathbf{h}(t+1)} = p_{\mathbf{h}(t)}$ . We then update the state of the Pauli frame and classical coefficients with the following update rules:

$$\begin{aligned} \mathcal{P}_{\text{PF}}^{(\mathbf{h}(t+1))} &= \mathcal{C}\mathcal{P}_{\text{PF}}^{(\mathbf{h}(t))}\mathcal{C}^{-1}\mathcal{P}_i\mathcal{P}_{\text{rec}}^{(t)} \\ s^{(\mathbf{h}(t+1))} &= \text{sgn}(\eta_i)s^{(\mathbf{h}(t))} \\ \gamma_Q^{(\mathbf{h}(t+1))} &= \gamma_Q\gamma_Q^{(\mathbf{h}(t))} \end{aligned} \quad (\text{E25})$$

Now, we can verify Eq. (E21) is satisfied in the  $(t+1)$ -th step if it is satisfied in the  $t$ -th step.

$$\begin{aligned} \sum_{\mathbf{h}(t+1)} q_{\mathbf{h}(t+1)} p_{\mathbf{h}(t+1)} \gamma_Q^{(\mathbf{h}(t+1))} s^{(\mathbf{h}(t+1))} \mathcal{P}_{\text{PF}}^{(\mathbf{h}(t+1))} \mathcal{U}_{\text{dev}}^{(\mathbf{h}(t+1))} &= \sum_{\mathbf{h}(t)} q_{\mathbf{h}(t)} p_{\mathbf{h}(t)} \gamma_Q^{(\mathbf{h}(t))} s^{(\mathbf{h}(t))} \mathcal{C}\mathcal{P}_{\text{PF}}^{(\mathbf{h}(t))}\mathcal{C}^{-1} \left( \sum_i \eta_i \mathcal{P}_i \right) \mathcal{N}\mathcal{C}\mathcal{U}_{\text{dev}}^{(\mathbf{h}(t))} \\ &= \mathcal{C} \sum_{\mathbf{h}(t)} q_{\mathbf{h}(t)} p_{\mathbf{h}(t)} \gamma_Q^{(\mathbf{h}(t))} s^{(\mathbf{h}(t))} \mathcal{P}_{\text{PF}}^{(\mathbf{h}(t))} \mathcal{U}_{\text{dev}}^{(\mathbf{h}(t))} \\ &= \mathcal{C}\tilde{\mathcal{U}}^{(t)} = \tilde{\mathcal{U}}^{(t+1)}. \end{aligned} \quad (\text{E26})$$

As we will see later, we can also construct a similar update rule of probabilistic error cancellation for a single qubit logical Pauli measurement; therefore, we can inductively show that decomposition specified with the update rule can satisfy Eq. (E21).

*c. Logical initialization and single-qubit logical Pauli measurement*

When code distances and magic-state distillation process are insufficient, there are not negligible errors also in the logical state preparation. These errors can be also assumed to be inserted stochastic logical Pauli noise maps just after initialization. We can consider that these preparations are ideal, and instead, there exists a virtual noisy idling operation just after initialization. We can mitigate these errors with the same update rules as the case of logical Clifford operations by treating these errors as decoding errors. Similarly, errors of single-qubit logical Pauli measurement are considered as a probabilistic logical bit-flip just before the logical measurement, and this can be processed in the same manner.

*d. Gate teleportation with magic state*

For applying  $T$ -gate by gate teleportation, we hope that we can perform the following process:

$$(\mathcal{I} \otimes \langle\langle \Pi_{\mathbf{x}} \rangle\rangle) \Lambda \mathcal{Q}_A \quad (\text{E27})$$

and then perform  $\mathcal{S}^{f(\mathbf{x})}$  depending on the measurement outcomes to indirectly achieve  $\mathcal{T}$  on the target system. However, in practice, what is performed until the measurement is

$$(\mathcal{I} \otimes \langle\langle \Pi_{\mathbf{x}} \rangle\rangle) \mathcal{N}\mathcal{P}_{\text{rec}}^{(t)} \Lambda (\mathcal{I} \otimes \mathcal{P}_{\text{PF}}^{(Q)}) \mathcal{Q}_A \quad (\text{E28})$$

where  $\mathcal{P}_{\text{rec}}^{(t)}$  is physical errors caused by logical magic state preparation, logical CNOT, and logical measurements. Compared to the case without QEM (Eq. E14), there is an additional logical Pauli noise  $\mathcal{N}$  that is caused by the failure of decoding to estimate  $\mathcal{P}_{\text{rec}}^{(t)}$ .

Since this procedure involves an intermediate measurement, we obtain the outcome  $\mathbf{x}$  randomly. The procedure for inverse decomposition is the same as that of logical Clifford operation: we calculate the inverse of the noise map  $\mathcal{N}^{-1} = \sum_i \eta_i \mathcal{P}_i$ , decompose a non-zero coefficient  $\eta_i$  as  $\eta_i = \gamma_Q \text{sgn}(\eta_i) q_i$  where  $\gamma_Q = \sum_i |\eta_i|$  and  $q_i = |\eta_i|/\gamma_Q$ . We remark that the measurement result  $\mathbf{x}$  is added to  $\mathbf{h}(t)$  together with the choice of QEM operation  $i$  to obtain  $\mathbf{h}(t+1)$ . Then,  $q_{\mathbf{h}(t)}$  is updated to  $q_{\mathbf{h}(t+1)} = q_i q_{\mathbf{h}(t)}$  and  $p_{\mathbf{h}(t+1)} = p_{\mathbf{x}} p_{\mathbf{h}(t)}$ , where  $p_{\mathbf{x}}$  is the probability that the measurement outcome is  $\mathbf{x}$ . Then, we can update the relevant elements with the following rules:

$$\begin{aligned}
\mathcal{U}_{\text{dev}}^{(\mathbf{h}^{(t+1)})} &= \frac{1}{p_{\mathbf{x}}} (\mathcal{S}^{f(\mathbf{x} \oplus \mathbf{y})} \otimes \langle \langle \Pi_{\mathbf{x}} | \rangle \rangle \mathcal{N} \mathcal{P}_{\text{rec}}^{(t)} \Lambda (\mathcal{I} \otimes \mathcal{P}_{\text{PF}}^{(Q)}) \mathcal{Q}_A \mathcal{U}_{\text{dev}}^{(\mathbf{h}^{(t)})}) \\
\mathcal{P}_{\text{PF}}^{(\mathbf{h}^{(t+1)})} &= \mathcal{S}^{f(\mathbf{x} \oplus \mathbf{y})} \text{Dis}_A [\mathcal{R}^{(\mathbf{h}^{(t)})}] \mathcal{S}^{-f(\mathbf{x} \oplus \mathbf{y})} \\
s^{(\mathbf{h}^{(t+1)})} &= \text{sgn}(\eta_i) s^{(\mathbf{h}^{(t)})} \\
\gamma_Q^{(\mathbf{h}^{(t+1)})} &= \gamma_Q \gamma_Q^{(\mathbf{h}^{(t)})},
\end{aligned} \tag{E29}$$

where

$$\begin{aligned}
\mathcal{R}^{(\mathbf{h}^{(t)})} &= \Lambda (\mathcal{P}_{\text{PF}}^{(\mathbf{h}^{(t)})} \otimes \mathcal{P}_{\text{PF}}^{(Q)}) \Lambda^{-1} \mathcal{P}_i \mathcal{P}_{\text{rec}}^{(t)}, \\
\mathbf{y} &= \text{mask}(\text{Dis}_\rho [\mathcal{R}^{(\mathbf{h}^{(t)})}]).
\end{aligned} \tag{E30}$$

Note that an additional decoding error map that de-

pends on whether we perform  $\mathcal{S}$  or not would occur after the delayed application of  $\mathcal{S}^{f(\mathbf{x} \oplus \mathbf{y})}$ . While this map is omitted for simplicity, we also perform probabilistic error cancellation for this map in the same way.

With the above update rules, we can verify Eq. (E21) is kept at the  $(t+1)$ -th step. The product of  $\mathcal{U}_{\text{dev}}^{(\mathbf{h}^{(t+1)})}$  and  $\mathcal{P}_{\text{PF}}^{(\mathbf{h}^{(t+1)})}$  is evaluated as follows:

$$\begin{aligned}
\mathcal{P}_{\text{PF}}^{(\mathbf{h}^{(t+1)})} \mathcal{U}_{\text{dev}}^{(\mathbf{h}^{(t+1)})} &= \frac{1}{p_{\mathbf{x}}} \mathcal{S}^{f(\mathbf{x} \oplus \mathbf{y})} \text{Dis}_A [\mathcal{R}^{(\mathbf{h}^{(t)})}] \mathcal{S}^{-f(\mathbf{x} \oplus \mathbf{y})} (\mathcal{S}^{f(\mathbf{x} \oplus \mathbf{y})} \otimes \langle \langle \Pi_{\mathbf{x}} | \rangle \rangle \mathcal{N} \mathcal{P}_{\text{rec}}^{(t)} \Lambda (\mathcal{I} \otimes \mathcal{P}_{\text{PF}}^{(Q)}) \mathcal{Q}_A \mathcal{U}_{\text{dev}}^{(\mathbf{h}^{(t)})}) \\
&= \frac{1}{p_{\mathbf{x}}} (\mathcal{S}^{f(\mathbf{x} \oplus \mathbf{y})} \otimes \langle \langle \Pi_{\mathbf{x}} | \rangle \rangle \text{Dis}_A [\mathcal{R}^{(\mathbf{h}^{(t)})}] \mathcal{N} \mathcal{P}_{\text{rec}}^{(t)} \Lambda (\mathcal{I} \otimes \mathcal{P}_{\text{PF}}^{(Q)}) \mathcal{Q}_A \mathcal{U}_{\text{dev}}^{(\mathbf{h}^{(t)})}) \\
&= \frac{1}{p_{\mathbf{x}}} (\mathcal{S}^{f(\mathbf{x} \oplus \mathbf{y})} \otimes \langle \langle \Pi_{\mathbf{x} \oplus \mathbf{y}} | \rangle \rangle \mathcal{R}^{(\mathbf{h}^{(t)})} \mathcal{N} \mathcal{P}_{\text{rec}}^{(t)} \Lambda (\mathcal{I} \otimes \mathcal{P}_{\text{PF}}^{(Q)}) \mathcal{Q}_A \mathcal{U}_{\text{dev}}^{(\mathbf{h}^{(t)})}) \\
&= \frac{1}{p_{\mathbf{x}}} (\mathcal{S}^{f(\mathbf{x} \oplus \mathbf{y})} \otimes \langle \langle \Pi_{\mathbf{x} \oplus \mathbf{y}} | \rangle \rangle \mathcal{P}_i \mathcal{N} \Lambda \mathcal{Q}_A \mathcal{P}_{\text{PF}}^{(\mathbf{h}^{(t)})}) \mathcal{U}_{\text{dev}}^{(\mathbf{h}^{(t)})}
\end{aligned} \tag{E31}$$

Therefore, an expectation value is evaluated as follows.

$$\begin{aligned}
&\sum_{\mathbf{h}^{(t+1)}} q_{\mathbf{h}^{(t+1)}} p_{\mathbf{h}^{(t+1)}} \gamma_Q^{(\mathbf{h}^{(t+1)})} s^{(\mathbf{h}^{(t+1)})} \mathcal{P}_{\text{PF}}^{(\mathbf{h}^{(t+1)})} \mathcal{U}_{\text{dev}}^{(\mathbf{h}^{(t+1)})} \\
&= \sum_{\mathbf{h}^{(t)}} \sum_{\mathbf{x}} q_{\mathbf{h}^{(t)}} p_{\mathbf{h}^{(t)}} \gamma_Q^{(\mathbf{h}^{(t)})} s^{(\mathbf{h}^{(t)})} (\mathcal{S}^{f(\mathbf{x} \oplus \mathbf{y})} \otimes \langle \langle \Pi_{\mathbf{x} \oplus \mathbf{y}} | \rangle \rangle (\sum_i \eta_i \mathcal{P}_i) \mathcal{N} \Lambda \mathcal{Q}_A \mathcal{P}_{\text{PF}}^{(\mathbf{h}^{(t)})}) \mathcal{U}_{\text{dev}}^{(\mathbf{h}^{(t)})} \\
&= \sum_{\mathbf{h}^{(t)}} \sum_{\mathbf{x}} q_{\mathbf{h}^{(t)}} p_{\mathbf{h}^{(t)}} \gamma_Q^{(\mathbf{h}^{(t)})} s^{(\mathbf{h}^{(t)})} (\mathcal{S}^{f(\mathbf{x} \oplus \mathbf{y})} \otimes \langle \langle \Pi_{\mathbf{x} \oplus \mathbf{y}} | \rangle \rangle \Lambda \mathcal{Q}_A \mathcal{P}_{\text{PF}}^{(\mathbf{h}^{(t)})}) \mathcal{U}_{\text{dev}}^{(\mathbf{h}^{(t)})} \\
&= \mathcal{T} (\sum_{\mathbf{x}} \langle \langle \Pi_{\mathbf{x} \oplus \mathbf{y}} | +_{\text{L}} \rangle \rangle) \sum_{\mathbf{h}^{(t)}} p_{\mathbf{x}} q_{\mathbf{h}^{(t)}} p_{\mathbf{h}^{(t)}} \gamma_Q^{(\mathbf{h}^{(t)})} s^{(\mathbf{h}^{(t)})} \mathcal{P}_{\text{PF}}^{(\mathbf{h}^{(t)})} \mathcal{U}_{\text{dev}}^{(\mathbf{h}^{(t)})} \\
&= \mathcal{T} \tilde{\mathcal{U}}^{(t)} = \tilde{\mathcal{U}}^{(t+1)}
\end{aligned} \tag{E32}$$

Therefore, we have verified the condition Eq. (E21) is satisfied for all the logical operations.

## Appendix F: On the noise model of decoding errors

In the manuscript, we used a noise model of decoding errors that can be modeled as Markovian and stochastic Pauli noise as Eq. (8). Here, we explain how this assumption is justified. First, we focus on whether we can treat an actual noise model as Markovian or not. When syndrome measurements may output a wrong value, we need successive  $d$  syndrome values for reliably estimat-

ing recovery operations. Since quantum states are in the logical code space only after recovery operations, actual quantum states are not in the code space during FTQC. This makes it hard to evaluate a logical noise map for several cycles during FTQC because this map does not take a logical state to another logical state, while we need to evaluate a logical noise map in advance for performing QEM on the code space. To avoid this problem, we assumed that the noise model defined by the following definition can well approximate the actual noise model. Suppose that we can perform perfect syndrome measurements in the  $ld$ -th cycle where  $l = 1, 2, \dots$  and can perform recovery operations just after that, a quantum state is in

the logical code space at the  $ld$ -th cycle. In this case, we can define a logical error map  $\mathcal{M}_{\text{dec}}$  from the  $(l-1)d$ -th cycle to the  $ld$ -th cycle. Here, we assume that if we have a logical operation  $\mathcal{U}$  which requires  $\chi d$  cycles, a logical map including effective decoding errors can be approximated with  $\mathcal{M}_{\text{dec}}^{\chi} \mathcal{U}$  when code distance  $d$  is sufficiently large. If this assumption holds, we can perform QEM for each logical operation for canceling noise map  $\mathcal{M}_{\text{dec}}^{\chi}$ . In the main text, although actual  $\chi$  depends on logical operations, we assume that  $\chi = 1$  for simplicity.

To verify that this assumption holds at least when physical errors are stochastic Pauli noise, we perform the following numerical analysis. Let  $\mathcal{M}_{\text{dec},c}$  be a noise map for  $c$ -cycle idling of a single logical qubit with code distance  $d$ , and let  $\Lambda^{(c)}$  be a Pauli transfer matrix of  $\mathcal{M}_{\text{dec},c}$ . Here,  $\mathcal{M}_{\text{dec},c}$  is a stochastic noise map since stochastic Pauli error can only cause logical Pauli errors, and thus  $\Lambda^{(c)}$  is a diagonal matrix. Our assumption can be rephrased as follows: There is an effective Pauli transfer matrix  $\Lambda_{\text{eff}}$  such that  $\Lambda^{(c)} = \Lambda_{\text{eff}}^c$  for sufficiently large  $c$ . Equivalently, we assume that each diagonal element decays exponentially to the number of cycles  $c$ . Since  $\Lambda_{00}$  is always unity for stochastic Pauli errors, we are interested in the other diagonal elements. Diagonal elements except  $\Lambda_{00}$  are shown according to the number of cycles in Fig. 10. We utilize the same settings as Sec. IV A 2, i.e., depolarizing noise map with  $p = 0.01$ . Note that  $\Lambda_{33}$  and  $\Lambda_{11}$  are equal since the behavior of surface codes is symmetric for Pauli- $X$  and  $Z$  errors. Numerical results are plotted with circle markers, and broken lines are fitting results with exponentially decaying function. We used data points with  $c > 20$  for fitting. Their behavior agrees well with our assumption except for the region where cycle count  $c$  is around 1. Thus, we can conclude that if a physical error is stochastic Pauli noise, we can define an effective logical noise map for each logical operation.

Next, we discuss the case when physical noise cannot be modeled as a stochastic Pauli. In practice, the noise of calibrated quantum operations is expected to be almost stochastic Pauli, since a unitary component in physical errors can be canceled by echoing. In addition, a noise map in a code space is well approximated as stochastic Pauli noise at a large distance [32]. Nevertheless, there may be non-negligible coherence in quantum noise. In this case, we can twirl this noise map and remove the unitary component of noise. We show that we can perform twirling on logical noise caused by logical Clifford operations if logical Pauli operations with physical operations, i.e., logical Pauli operations without updating Pauli frame, can be achieved with negligible error rates. Note that logical error rates caused by logical Pauli operations are expected to be sufficiently small compared with those by logical Clifford operations. This is because logical Pauli operations can be performed with transversal single-qubit operations completed in a single cycle, and errors caused by these operations are negligible compared with those by two-qubit operations for stabilizer

measurements. Suppose that we perform logical Clifford operation  $\mathcal{C}$  and a logical noise map  $\mathcal{M}_{\text{dec}}^{\chi}$  follows it, and we perform twirling noise  $\mathcal{M}_{\text{dec}}^{\chi}$  with a set of Pauli operators  $\mathbb{S}$ . Then, the twirling process can be described as follows:

$$\left( \frac{1}{|\mathbb{S}|} \sum_{\mathcal{P} \in \mathbb{S}} \mathcal{P} \mathcal{M}_{\text{dec}}^{\chi} \mathcal{P} \right) \mathcal{C} = \frac{1}{|\mathbb{S}|} \sum_{\mathcal{P} \in \mathbb{S}} \mathcal{P} \mathcal{M}_{\text{dec}}^{\chi} \mathcal{C} (\mathcal{C}^{\dagger} \mathcal{P} \mathcal{C}), \quad (\text{F1})$$

where  $\mathcal{P}$  is a superoperator of logical Pauli operations. Since  $\mathcal{C}^{\dagger} \mathcal{P} \mathcal{C}$  is a logical Pauli operation, twirling of  $\mathcal{M}_{\text{dec}}^{\chi}$  can be done only with logical Pauli operations. We can make the same arguments for Pauli measurements and feedback operations dependent on their outcomes. Since all the elemental logical operations except for magic state injection are Clifford operations or Pauli channels, we can apply Pauli twirling to most of the quantum operations in FTQC. Note that while logical Pauli operations for computation can be done by updating a Pauli frame, logical Pauli operations for twirling requires physical implementation on quantum devices. This is because logical Pauli operations by updating a Pauli frame must be tracked after every successive logical operation that we take into account. For example, when we consider general noise  $\mathcal{M}_{\text{dec}}^{\chi}$ , which is not necessarily stochastic Pauli noise, an operator  $P' = \mathcal{M}_{\text{dec}}^{\chi} \mathcal{P} \mathcal{M}_{\text{dec}}^{\chi}$  is not a Pauli operator in general, and thus we cannot continue tracking a frame as a Pauli operator. Thus the Pauli twirling must be done physically.

### Appendix G: Details of numerical analysis

In this Appendix, we describe details of numerical simulations in this paper. First, we describe numerical simulations for evaluating decoding errors. In the simulation, we adopt a uniform depolarizing noise model, which occurs on each physical qubit independently and acts as follows:

$$\mathcal{E}(\rho) = (1-p)\rho + \frac{p}{3}(X\rho X + Y\rho Y + Z\rho Z). \quad (\text{G1})$$

This error acts on data qubits at the beginning of each cycle and acts on ancillary qubits just before its measurement. As shown in the main text, we assume perfect syndrome measurements at the 0-th and  $d$ -th cycles, which guarantees that quantum states at these cycles are in logical space with recovery operations regardless of whether decoding is successful or not. Then, we evaluate logical error probabilities during these cycles. For estimating a recovery operation, we used minimum-weight perfect matching decoder [40]. This decoder reduces the decoding problem to an instance of a minimum-weight perfect matching problem. While this problem is NP-hard when there are Pauli- $Y$  errors, we can approximately solve this problem by using Edmonds' blossom algorithm [41]. It is known that surface codes show threshold behavior even with this approximation. We use an implementation in

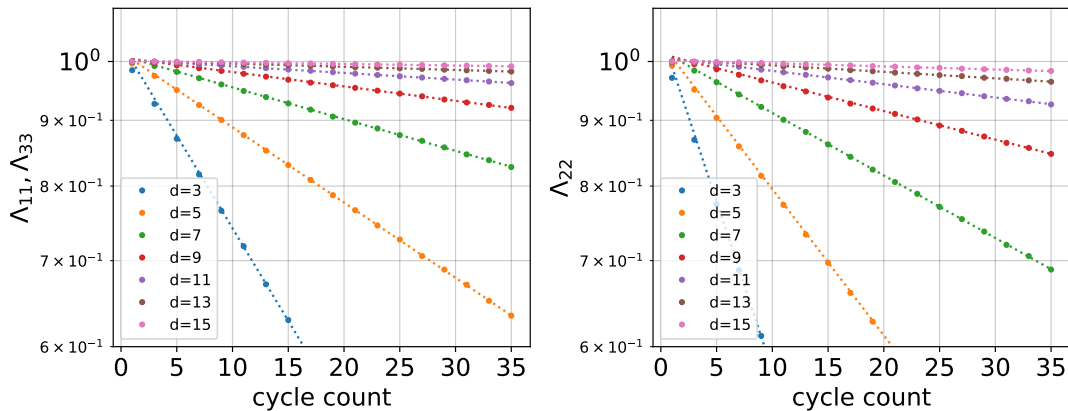


FIG. 10. Diagonal elements of Pauli-transfer matrix for a noise map of a single logical qubit during  $c$  syndrome-measurement cycles are plotted according to the code cycles. Each color corresponds to the code distance of a logical qubit. Numerical results are plotted with circle markers, and broken lines are fitting results with exponentially decaying function.

Ref. [60] for solving this problem. To estimate the logical error rate, we evaluate  $10^5$  samples for each data point in Fig. 3(b) and  $10^6$  samples for the other figures.

In the performance evaluation of error mitigation for decoding errors, we assume an error channel for each logical gate is a non-uniform logical depolarizing channel obtained in the benchmark of logical error probabilities in surface codes. Since there is no perfect syndrome measurement in practice, this assumption does not hold exactly. Nevertheless, this approximation is asymptotically correct, and thus we employed this assumption to evaluate the performance of QEM for logical errors.

For the simulation of Clifford circuits, we used a stabilizer circuit simulator of which the memory allocations are optimized so that updates for actions of Clifford operations become sequential. With this technique, simulation of stabilizer circuits dominated by Clifford opera-

tions rather than Pauli measurements becomes hundreds of times faster than the existing implementation stabilizer simulators [42].

For Solovay-Kitaev algorithm, we use a method and implementation proposed and published in Ref. [35]. While we need to limit the allowed number of  $T$ -gates, this method outputs a sequence of Clifford and  $T$ -gates according to an allowed error rate  $\varepsilon$ . Thus, we searched the minimum error rate  $\varepsilon^*$  with which the algorithm outputs a sequence with the number of  $T$ -gates smaller than the allowed number of  $T$ -gates. This search is done with a simple bisection method and repeated until accuracy reaches  $10^{-14}$ . For the simulation of SWAP test circuits, we use Qulacs [61], which is a simulator for general noisy quantum circuits and is fast especially when we perform a huge number of simulations of small quantum circuits.

- 
- [1] P. W. Shor, SIAM review **41**, 303 (1999).  
[2] A. W. Harrow, A. Hassidim, and S. Lloyd, Physical review letters **103**, 150502 (2009).  
[3] M. A. Nielsen and I. Chuang, “Quantum computation and quantum information,” (2002).  
[4] D. A. Lidar and T. A. Brun, *Quantum error correction* (Cambridge University Press, 2013).  
[5] A. G. Fowler, M. Mariantoni, J. M. Martinis, and A. N. Cleland, Physical Review A **86**, 032324 (2012).  
[6] C. Horsman, A. G. Fowler, S. Devitt, and R. Van Meter, New Journal of Physics **14**, 123011 (2012).  
[7] A. G. Fowler and C. Gidney, arXiv preprint arXiv:1808.06709 (2018).  
[8] I. D. Kivlichan, C. Gidney, D. W. Berry, N. Wiebe, J. McClean, W. Sun, Z. Jiang, N. Rubin, A. Fowler, A. Aspuru-Guzik, *et al.*, Quantum **4**, 296 (2020).  
[9] J. O’Gorman and E. T. Campbell, Physical Review A **95**, 032338 (2017).  
[10] K. Temme, S. Bravyi, and J. M. Gambetta, Physical review letters **119**, 180509 (2017).  
[11] Y. Li and S. C. Benjamin, Physical Review X **7**, 021050 (2017).  
[12] S. Endo, S. C. Benjamin, and Y. Li, Physical Review X **8**, 031027 (2018).  
[13] J. Sun, X. Yuan, T. Tsunoda, V. Vedral, S. C. Benjamin, and S. Endo, arXiv preprint arXiv:2001.04891 (2020).  
[14] S. McArdle, X. Yuan, and S. Benjamin, Physical review letters **122**, 180501 (2019).  
[15] X. Bonet-Monroig, R. Sagastizabal, M. Singh, and T. O’Brien, Physical Review A **98**, 062339 (2018).  
[16] Z. Cai, arXiv preprint arXiv:2007.01265 (2020).  
[17] A. Strikis, D. Qin, Y. Chen, S. C. Benjamin, and Y. Li, arXiv preprint arXiv:2005.07601 (2020).  
[18] P. Czarnik, A. Arrasmith, P. J. Coles, and L. Cincio, arXiv preprint arXiv:2005.10189 (2020).  
[19] S. Endo, Z. Cai, S. C. Benjamin, and X. Yuan, arXiv preprint arXiv:2011.01382 (2020).  
[20] A. Peruzzo, J. McClean, P. Shadbolt, M.-H. Yung, X.-Q.

- Zhou, P. J. Love, A. Aspuru-Guzik, and J. L. O'Brien, *Nature communications* **5**, 1 (2014).
- [21] A. Kandala, A. Mezzacapo, K. Temme, M. Takita, M. Brink, J. M. Chow, and J. M. Gambetta, *Nature* **549**, 242 (2017).
- [22] J. R. McClean, J. Romero, R. Babbush, and A. Aspuru-Guzik, *New Journal of Physics* **18**, 023023 (2016).
- [23] M. Cerezo, A. Arrasmith, R. Babbush, S. C. Benjamin, S. Endo, K. Fujii, J. R. McClean, K. Mitarai, X. Yuan, L. Cincio, *et al.*, arXiv preprint arXiv:2012.09265 (2020).
- [24] K. Bharti, A. Cervera-Lierta, T. H. Kyaw, T. Haug, S. Alperin-Lea, A. Anand, M. Degroote, H. Heimonen, J. S. Kottmann, T. Menke, *et al.*, arXiv preprint arXiv:2101.08448 (2021).
- [25] A. Y. Kitaev, *Russian Mathematical Surveys* **52**, 1191 (1997).
- [26] C. M. Dawson and M. A. Nielsen, arXiv preprint quant-ph/0505030 (2005).
- [27] R. Blume-Kohout, J. K. Gamble, E. Nielsen, J. Mizrahi, J. D. Sterk, and P. Maunz, arXiv preprint arXiv:1310.4492 (2013).
- [28] D. Greenbaum, arXiv preprint arXiv:1509.02921 (2015).
- [29] D. Gottesman, arXiv preprint quant-ph/9705052 (1997).
- [30] B. Eastin and E. Knill, *Physical review letters* **102**, 110502 (2009).
- [31] L. Rieseboos, X. Fu, S. Varsamopoulos, C. G. Almudever, and K. Bertels, in *Proceedings of the 54th Annual Design Automation Conference 2017* (2017) pp. 1–6.
- [32] S. Bravyi, M. Englbrecht, R. König, and N. Peard, *npj Quantum Information* **4**, 1 (2018).
- [33] N. C. Jones, R. Van Meter, A. G. Fowler, P. L. McMahon, J. Kim, T. D. Ladd, and Y. Yamamoto, *Physical Review X* **2**, 031007 (2012).
- [34] A. G. Fowler, A. C. Whiteside, and L. C. Hollenberg, *Physical review letters* **108**, 180501 (2012).
- [35] N. J. Ross and P. Selinger, arXiv preprint arXiv:1403.2975 (2014).
- [36] E. Campbell, *Physical review letters* **123**, 070503 (2019).
- [37] S. Endo, I. Kurata, and Y. O. Nakagawa, *Physical Review Research* **2**, 033281 (2020).
- [38] C. Wang, J. Harrington, and J. Preskill, *Annals of Physics* **303**, 31 (2003).
- [39] N. Delfosse and N. H. Nickerson, arXiv preprint arXiv:1709.06218 (2017).
- [40] E. Dennis, A. Kitaev, A. Landahl, and J. Preskill, *Journal of Mathematical Physics* **43**, 4452 (2002).
- [41] J. Edmonds, *Canadian Journal of mathematics* **17**, 449 (1965).
- [42] S. Aaronson and D. Gottesman, *Physical Review A* **70**, 052328 (2004).
- [43] A. K. Ekert, C. M. Alves, D. K. Oi, M. Horodecki, P. Horodecki, and L. C. Kwek, *Physical review letters* **88**, 217901 (2002).
- [44] S. Lloyd, *Science*, 1073 (1996).
- [45] D. W. Berry, A. M. Childs, R. Cleve, R. Kothari, and R. D. Somma, *Physical review letters* **114**, 090502 (2015).
- [46] G. H. Low and I. L. Chuang, *Quantum* **3**, 163 (2019).
- [47] G. H. Low and I. L. Chuang, *Physical review letters* **118**, 010501 (2017).
- [48] S. Endo, Q. Zhao, Y. Li, S. Benjamin, and X. Yuan, *Physical Review A* **99**, 012334 (2019).
- [49] A. C. Vazquez, R. Hiptmair, and S. Woerner, arXiv preprint arXiv:2009.04484 (2020).
- [50] K. Mitarai and K. Fujii, arXiv preprint arXiv:1909.07534 (2019).
- [51] K. Mitarai and K. Fujii, arXiv preprint arXiv:2006.11174 (2020).
- [52] J. R. McClean, Z. Jiang, N. C. Rubin, R. Babbush, and H. Neven, *Nature Communications* **11**, 1 (2020).
- [53] J. R. McClean, M. E. Kimchi-Schwartz, J. Carter, and W. A. De Jong, *Physical Review A* **95**, 042308 (2017).
- [54] S. B. Bravyi and A. Y. Kitaev, arXiv preprint quant-ph/9811052 (1998).
- [55] B. J. Brown, K. Laubscher, M. S. Kesselring, and J. R. Wootton, *Physical Review X* **7**, 021029 (2017).
- [56] C. Gidney and A. G. Fowler, *Quantum* **3**, 135 (2019).
- [57] A. Holmes, M. R. Jokar, G. Pasandi, Y. Ding, M. Pedram, and F. T. Chong, arXiv preprint arXiv:2004.04794 (2020).
- [58] Y. Li, *New Journal of Physics* **17**, 023037 (2015).
- [59] C. J. Trout and K. R. Brown, *International Journal of Quantum Chemistry* **115**, 1296 (2015).
- [60] V. Kolmogorov, *Mathematical Programming Computation* **1**, 43 (2009).
- [61] Y. Suzuki, Y. Kawase, Y. Masumura, Y. Hiraga, M. Nakadai, J. Chen, K. M. Nakanishi, K. Mitarai, R. Imai, S. Tamiya, *et al.*, arXiv preprint arXiv:2011.13524 (2020).